International Journal of Environmental Research (2021) 15:1017–1036
https://doi.org/10.1007/s41742-021-00368-4

RESEARCH PAPER

Hexavalent Chromium Removal Using Ionic Liquid Coated Magnetic Nano Zero-Valent Iron Biosynthesized by *Camellia sinensis* Extract

Saber Mousazadeh[1] · Shahab Shariati[2] · Mohammad Yousefi[3] · Sahar Baniyaghoob[1] · Hassan Kefayati[2]

Received: 4 August 2021 / Revised: 23 August 2021 / Accepted: 31 August 2021 / Published online: 7 September 2021

Abstract

Nano zero-valent iron (nZVI) coated with magnetite and an imidazolium-based ionic liquid (1-hexyl-3-methylimidazolium hexafluorophosphate (HMIMPF$_6$)) core/shell nanoparticles (NPs) (nZVI@Fe$_3$O$_4$@HMIMPF$_6$) were successfully green synthesized for the first time using industrial iron waste. Polyphenols were extracted from dried leaves of *Camellia sinensis* and applied as the reducing agent for nZVI synthesis. Synthesized NPs were characterized by FT-IR, XRD, VSM, BET, SEM, TEM, and mapping analysis. According to the results, NPs were in the size range of less than 30 nm and the values of $a_{s,\,\mathrm{BET}} = 3.5975\ \mathrm{m^2 g^{-1}}$, V_m (BET monolayer capacity) $= 0.8265\ \mathrm{cm^3 (STP)\, g^{-1}}$, $C = 47.378$, total pore volume $(\frac{p}{p^0} = 0.990) = 0.14998\ \mathrm{cm^3 g^{-1}}$ and mean pore diameter =16.68 nm were obtained. These NPs were used for the Cr (VI) removal from aqueous samples. Taguchi orthogonal array design was used to optimize the various affecting variables on the efficiency of Cr (VI) removal. Results showed that about 90.0% of Cr (VI) were removed at the optimum conditions. Kinetic and isotherm studies were conducted, and the pseudo-second order kinetic model was determined as the most appropriate kinetic model. The equilibrium data displayed proper linearity with the Freundlich isotherm model ($R^2 = 0.9697$), and the maximum adsorption capacity was found to be 56.49 mg g^{-1}(in terms of CrO$_4{}^{2-}$ ions). Also, Redlich-Peterson, Sips, and Toth as three-parameter isotherm models were compared to two-parameter models using MATLAB's fmincon function. Thermodynamic studies showed negative $\Delta G°$, $\Delta H° = 50.255$ kJ mol^{-1}, and $\Delta S° = +0.1799$ kJ mol^{-1} K^{-1} indicating spontaneous and endothermic adsorption process. According to the results, the nZVI@Fe$_3$O$_4$@IL NPs can be recovered by an external magnet and exhibit good applicability for Cr (VI) removal from real samples.

✉ Shahab Shariati
shariaty@iaurasht.ac.ir

[1] Department of Chemistry, Science and Research Branch, Islamic Azad University, Tehran, Iran

[2] Department of Chemistry, Rasht Branch, Islamic Azad University, Rasht, Iran

[3] Department of Chemistry, Faculty of Pharmaceutical Chemistry, Tehran Medicine Sciences, Islamic Azad University, Tehran, Iran

Graphic Abstract

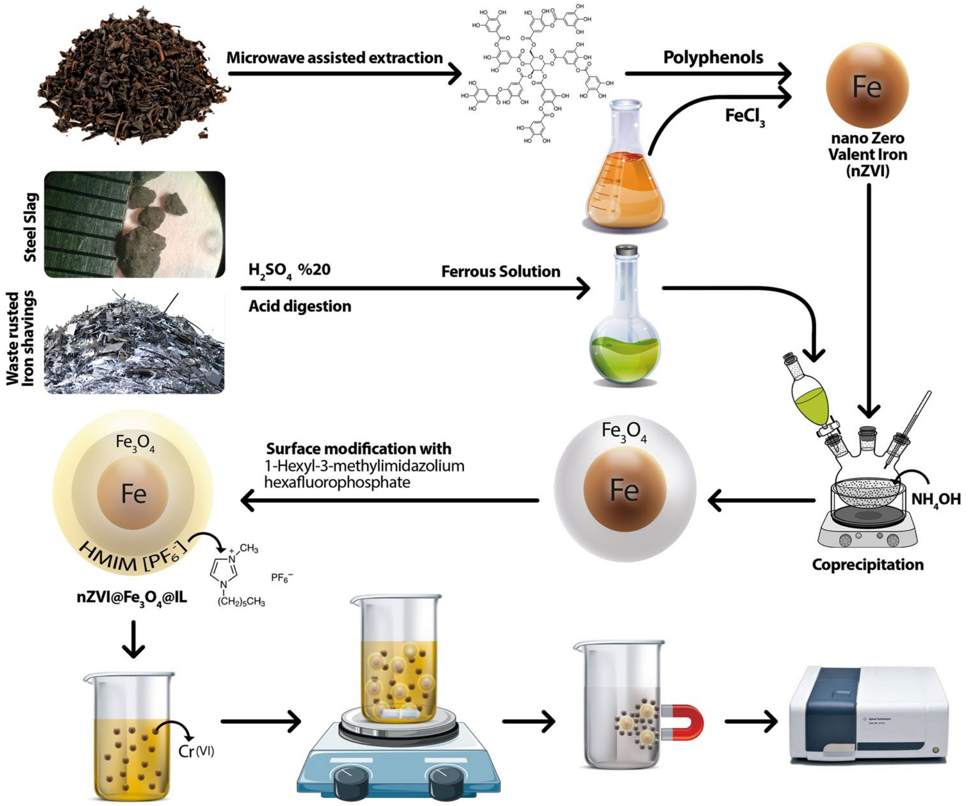

Article Highlights

- **Core-shell structures of nZVI@Fe_3O_4@IL were synthesized for the first time**
- **Steel slag and waste rusted iron shavings were used as ferrous ion sources**
- **Polyphenols were extracted from *Camellia sinensis* and used for biosynthesis of nZVI**
- **The obtained NPs were used for the removal of Cr (VI) ions from aqueous samples**
- **Two and three parameter isotherm models, kinetic and thermodynamic studies were investigated**

Keywords Adsorption · *Camellia sinensis* · Hexavalent chromium · Magnetic nanoparticles · Microwave-assisted extraction · Nano zero-valent iron

Introduction

Chromium is an active transition metal with several applications in many industrial processes. The tri and hexavalent chromium are the most stable oxidation states. Due to the pH, hexavalent chromium (Cr (VI)) species may have different forms in the aqueous solution like dichromate ($Cr_2O_7^{2-}$), dichromic acid ($H_2Cr_2O_7$) or chromate (CrO_4^{2-}) (Kim et al. 2012). Cr (III) is required for human and animal nutrition, while the toxicity and carcinogenicity of the Cr (VI) species are reported (Oliveira 2012). CrO_4^{2-} is toxic because of its ability to penetrate in cellular membranes, which is reduced to the Cr (V), Cr (IV), and Cr (III) and may affect cellular proteins, lipids, and DNA by generating reactive oxygen species (Mitra et al. 2017). The World Health Organization (WHO) recommended 50 µg L^{-1} as the maximum allowable concentration for entire chromium species (Zhang et al. 2020).

Researchers have developed various techniques for Cr (VI) removal like photocatalysis (Wang et al. 2004), precipitation (Peng et al. 2005), membrane technology (Daraei et al. 2014), ion exchange (Xing et al. 2007), and adsorption (Bishnoi et al. 2004). The adsorption method is the most convenient method for this purpose since it is cost-effective, easy to use, and efficient (Ali and Gupta 2006). Different adsorbents have been synthesized for this manner, such as carbon nanotubes (Abbas et al. 2016), clay minerals (Gu et al. 2019), layered double hydroxides (Gong et al. 2011), nano metal oxides (Hua et al. 2012), activated carbon (Karnib et al. 2014), carbon film (Huang et al. 2018), ordered mesoporous (Barczak et al. 2015) and graphene oxides (Zhang et al. 2015). In addition to the low sorption capacity of conventional adsorbents, subsequent separation from the aqueous solution is a major problem (Liu et al. 2008).

Surface-modified nZVI particles have shown significant potential for environmental applications (Stefaniuk et al. 2016). Fe_3O_4 coating could enhance nZVI magnetic properties and protects nZVI from oxidation and agglomeration.

nZVI can be achieved by several procedures such as milling (Li et al. 2009), carbothermal reaction (Nisticò and Carlos 2019), ultrasound-assisted (Jamei et al. 2014), electrochemical deposition (Yoo et al. 2007), and green processes (Fazlzadeh et al. 2017). Green synthesis of nZVI includes the extraction of polyphenols from plants. Polyphenols are reducing agents that have been used instead of conventional and toxic materials like $NaBH_4$ (Li and Jiang 2010).

Although there have been many studies on Cr (VI) removal, this is the first time that ionic liquid (IL) modified nZVI@Fe_3O_4 core/shell structures are applied for this purpose. ILs are liquids entirely composed of ions. ILs are well known for their negligible vapor pressure, high electrochemical and thermal stability, high ionic conductivity, good solubility, and tunable viscosity and structures (He and Alexandridis 2017). Having these qualities presents ILs as an appropriate replacement for convenient organic solvents. A combination of ILs and NPs can generate cationic/anionic ion layers all over the NPs, given electrostatic forces (Sakai et al. 2015). ILs coated NPs exhibit better dispersibility and thermostability (Fukushima and Aida 2007). 1-Hexyl-3-methylimidazolium hexafluorophosphate (HMIMPF6) is a water-immiscible room temperature ionic liquid (RTIL) with an imidazolium-type cation (Du et al. 2018). HMIMPF6 has been known as an extraction solvent for Cr (VI) evaluation in the aqueous solution (Chen et al. 2010).

There is no report on using steel slag as an iron source for magnetite synthesis and also using $HMIMPF_6$ IL for surface modification. This work aims to extract polyphenols from *Camellia sinensis* as a reducing agent for nZVI synthesis. nZVI particles were coated with Fe_3O_4 by the co-precipitation route. The ferrous solutions were prepared by acid digestion of steel slag and waste rusted iron shavings. Finally, the core/shell surface was modified with HMIMPF6. Moreover, it was applied for Cr (VI) removal from aqueous solutions. The Taguchi method was applied to optimize affecting factors on the removal efficiency. In addition to kinetic and isotherm studies, the thermodynamic parameters were also evaluated for the adsorption process.

Experimental

Chemicals

The chemicals including iron(III) chloride hexahydrate ($FeCl_3.6H_2O$), iron(II) chloride tetrahydrate ($FeCl_2.4H_2O$), ammonia (NH_3, 25% *w*/*w*), H_2SO_4 (98% *w*/*w*), HCl (37% *w*/*w*), absolute ethanol, sodium hydroxide, 1-hexyl-3-methylimidazolium hexafluorophosphate ($HMIMPF_6$), ammonium iron (II) sulfate hexahydrate, hydroxylamine hydrochloride, 1,10-phenanthroline and sodium acetate were obtained from Sigma-Aldrich (ST. Louise, Missouri, USA), Merck (Darmstadt, Germany) and Fluka (Buchs, Switzerland). Potassium chromate (K_2CrO_4, analytical grade, Sigma-Aldrich) was used to prepare Cr (VI) stock solution (1000 mg L^{-1}). All working solutions were prepared with diluting this stock solution with deionized water.

Instruments and Apparatus

A Philips X-ray diffraction (XRD, Model PW1730, Netherlands) using CuK_α with a 2θ range of 5°–80° was applied to characterize the synthesized nZVI@Fe_3O_4@IL NPs. Fourier transform infrared (FT-IR) spectra were conducted on a Shimadzu Fourier transform infrared spectrometer (model 8900, Japan) in the range of 400–4000 cm^{-1}. A Philips scanning electron microscopy (SEM, model XL30, Netherlands) was utilized to investigate the surface of NPs. For UV–Vis measurements, an Agilent spectrophotometer (model Cary 60, USA) was employed. WTW pH meter (model 7110, Germany) was used to determine the pH of solutions. Also, a Hitachi transmission electron microscope (TEM, Model H9500, Japan) was applied to determine the size of prepared NPs with an accelerating voltage of 100 kV. A vibrating sample magnetometer (VSM; MDKFD, Iran) was utilized to evaluate the magnetic property of the synthesized NPs. LMS sorption analyzer (model BELSORP-mini II, Singapore) was applied to conduct N_2 adsorption–desorption experiments at 77 K. A 1.4 T permanent magnet was used to separate magnetic NPs from solutions (1 × 3 × 5 cm).

Preparation of nZVI@Fe_3O_4@IL NPs

Acid Digestion of Industrial Waste

The ferrous solutions were prepared by acid digestion of steel slag and waste rusted iron shavings. Briefly, 5 g steel slag and waste rusted iron shavings were separately added to different beakers, and 100 mL of sulfuric acid (20%) was added to each beaker, and the mixtures were heated at 80 °C for 24 h. Subsequently, the green solution of ferrous ion was separated from sediment by Büchner filtration.

For measuring the iron concentration in digested solutions, the spectrophotometric method based on 1,10-phenanthroline was applied. In this method, the absorbance of the reddish/orange ferrous- 1,10-phenanthroline complex is determined at 512 nm. For this purpose, 1.0, 2.0, 5.0, 10.0, and 25.0 mL of ferrous ammonium sulfate hexahydrate solution ($(NH_4)_2Fe(SO_4)_2.6H_2O$, 10 mg L^{-1}) were added into a series of 100 mL volumetric flux. After that, 1 mL hydroxylamine hydrochloride (10% *w*/*v*), 5 mL 1,10-phenanthroline (1000 mg L^{-1}), and 8 mL sodium acetate (10% *w*/*v*) solutions were added, and the obtained combination was diluted to 100 mL with distilled water to form iron (II) standard solutions. Also, unknown samples were prepared by adding 2 mL of digested solution in the same way as the standard solutions. After absorbance measurement with a spectrophotometer, the iron concentration in the digested solutions of steel slag and waste rusted iron shavings were determined as 178 and 143 mg L^{-1}, respectively.

Microwave-Assisted Extraction of Polyphenols from *Camellia sinensis*

Polyphenols as reducing agents were extracted from *Camellia sinensis* dried leaves (producing area: Guilan, Iran). For this purpose, the available microwave-assisted procedure was modified and then applied (Spigno and De Faveri 2009). Primarily, 10 g black tea was mixed with 200 mL of deionized (DI) water/ethanol solution (1:1), and the suspension was left for 90 min at room temperature (r.t). Afterward, the suspension was irradiated with microwaves for 4 min at 720 W for 45 s power on and 10 s power off for five times, and finally power on (15 s).

Synthesis of nZVI@Fe_3O_4@IL Core/Shell NPs

For the synthesis of nZVI, the iron (III) chloride solution was mixed with the extract (1:4 *v*/*v*). Resulted particles were centrifuged and then rinsed multiple times with a 1:1 solution of DI/ethanol. The synthesized NPs showed no magnetic effect with a super magnet. After that, the NPs were kept in pure ethanol for the next step.

The co-precipitation process was applied for nZVI@Fe_3O_4 NPs preparation (Khabazipour et al. 2016). Briefly, 4.0 g nZVI from the previous step was dispersed in 250 mL ammonia solution (4.5 M) in a three-neck flask and the mixture temperature was increased to 80 °C. After that, from a separately funnel, 50 mL ferrous solution produced from the digestion of steel slag was added dropwise at 80 °C to the mixture in the three-neck flask. Due to the oxidation of magnetite particles in the presence of oxygen, the dissolved oxygen was removed by purging nitrogen gas during the precipitation step. Then, synthesized NPs were washed three times with 250 mL of NaOH solution (0.1 M) and dried at 85 °C (24 h).

For surface modification with $HMIMPF_6$ IL, 1 g of obtained NPs from the previous step was added to the solutions containing 4–15% (*v*/*v*) $HMIMPF_6$ in chloroform (Chen et al. 2012). The mixture was stirred at r.t until complete evaporation of chloroform (5 h). Figure 1 summarizes the NPs synthesis procedure.

Adsorption Experiments

The nZVI@Fe_3O_4@IL NPs were applied to refine Cr (VI) solutions. In this work, five affecting experimental factors were optimized at four levels by Taguchi fractional factorial design. The Taguchi orthogonal array design is a statistical and powerful method for optimizing of affecting parameters (Toutounchi et al. 2019). Experimental factors including solution pH (2–7), adsorbent dose (0.05–0.12 g), contact time (5–45 min), ionic liquid (4–15%) and ionic strength (0–0.05 M), were studied to find the optimum values and to assess their contribution in the removal of Cr (VI) ions by the prepared nZVI@Fe_3O_4@IL NPs. According to the number of control factors, the OA_{16} design (Dai et al. 2009) was applied and 16 experiments were suggested for optimizing the process that were repeated for two times and the mean of two responses were used for ANOVA calculations (Table 1).

All experiments were performed with 25 mL solutions containing 40 mg L^{-1} CrO_4^{2-} ions at r.t. Upon completion of the removal experiments, a permanent super magnet was applied to separate the NPs. A spectrophotometer was utilized at 370 nm to measure CrO_4^{2-} concentrations of the solutions after the adsorption process using a proper calibration curve. The amount of adsorbed CrO_4^{2-} ions was calculated as follows (Eq. 1):

$$\%\ \text{Removal} = \frac{C_0 - C_t}{C_0} \times 100, \tag{1}$$

where C_0 and C_t are the initial and equilibrium concentrations of CrO_4^{2-} ions, respectively. The optical absorbance of different standard solutions of Cr (VI) (as CrO_4^{2-} ion, 5–100 mg L^{-1}) was measured at 370 nm, and the resulted calibration curve exhibited a linear relationship ($R^2=0.999$) at pH 2. To investigate the reusability of synthesized adsorbent, the NPs were washed with 3 mL of 0.1 M NaOH solution, and the excessive NaOH was washed out from NPs with DI and finally dried in an oven at 40 °C.

pH_{pzc} Determination for nZVI@Fe_3O_4@IL NPs

The point of zero charge (pH_{pzc}) is the pH of the mixture at which the net charge on the surface of NPs equals zero

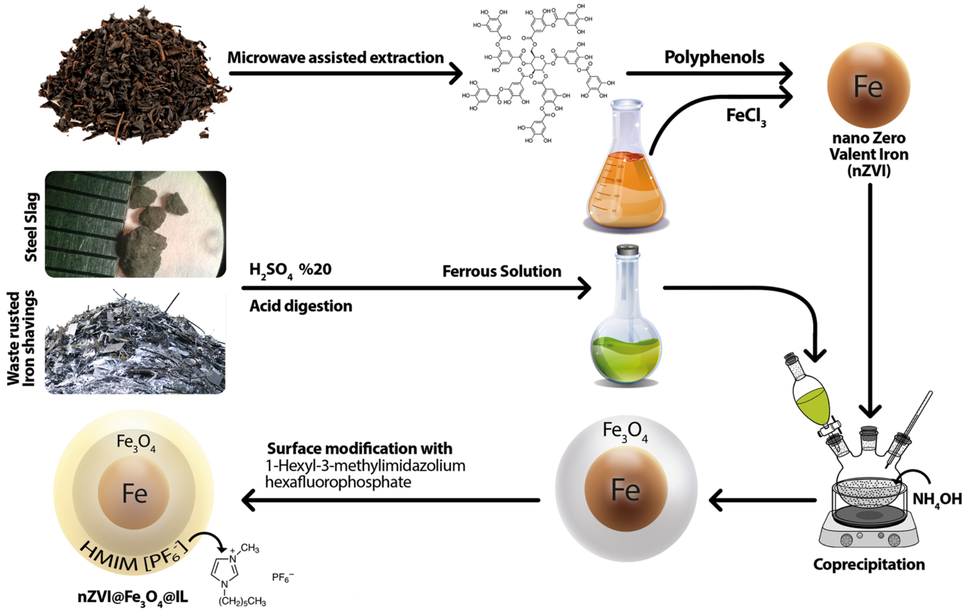

Fig. 1 Schematic for the preparation of nZVI@Fe3O4@IL

Table 1 OA$_{16}$ matrix for Cr (VI) removal experiments

Exp. no	Time (min)	Ionic strength (M)	Adsorbent weight (g)	pH	Ionic liquid (%)	Removal efficiency (%)
1	5	0	0.05	2	4	88
2	15	0.005	0.07	2	7	91
3	30	0.01	0.1	2	10	87
4	45	0.05	0.12	2	15	92
5	30	0.005	0.05	3.5	15	81
6	45	0	0.07	3.5	10	89
7	5	0.05	0.1	3.5	7	88
8	15	0.01	0.12	3.5	4	93
9	45	0.01	0.05	5	7	63
10	30	0.05	0.07	5	4	90
11	15	0	0.1	5	15	73
12	5	0.005	0.12	5	10	93
13	15	0.05	0.05	7	10	63
14	5	0.01	0.07	7	15	55
15	45	0.005	0.1	7	4	78
16	30	0	0.12	7	7	82

(Mustafa et al. 2013). In this study, the pH drift method was applied for measuring pH$_{pzc}$ value for the synthesized nZVI@Fe$_3$O$_4$@IL NPs. The pH drift method is preferred over the titration method due to fewer steps, standard apparatus, and time-saving (Pashai Gatabi et al. 2016). For this purpose, 50 mL of 0.1 M NaOH solutions were added into the nine separate beakers with the same size. 0.1 M NaOH and 0.1 M HCl solutions were used to adjust pH values between 2 and 10 (pH$_{initial}$). Then, 0.03 g nZVI@Fe$_3$O$_4$@IL NPs were mixed with the solutions and magnetically stirred at 250 rpm at r.t. The final pH (pH_{final}) of solutions was measured after 48 h. The intersection point of the curve resulted from the plot of pH_{final} vs $pH_{initial}$ values with the $pH_{initial} = pH_{final}$ line, gives pH_{pzc}.

Results and Discussions

Structural Characterization

The FT-IR spectra of synthesized (a) nZVI; (b) nZVI@Fe_3O_4; (c) nZVI@Fe_3O_4@IL NPs were shown in Fig. 2. In the nZVI spectra (Fig. 2a) the absorption bands at 1693 and 3467 cm^{-1} are related to the –COO and –OH groups due to forming the FeOOH layer on the nZVI surface. Bands at about 3000 and 1084 cm^{-1} are assigned to aromatic –C–H and C–O–C groups of tea extract, respectively. Figure 2b shows the FT-IR spectra of nZVI@Fe_3O_4. The bands at 3410 and 1629 cm^{-1} are ascribed to the –OH and –COO, respectively. Also, bands between 400 and 600 cm^{-1} represent the formation of Fe–O metal oxides (Danesh et al. 2019). Two bands at 618 and 466 cm^{-1} are related to the stretching vibrations of Fe^{3+}–O^{2-} spinel structure with tetrahedral and octahedral sites. The typical bands for nZVI@Fe_3O_4@IL (Fig. 2c) at 3050, 2962, and 2869 are attributed to the stretching vibrations of aromatic and aliphatic -CH groups. Also, bands at 3173, 1629, 1571, and 1430 cm^{-1} belong to the N–H, –COO, –C = N, and C = C groups in the phenolic ring and IL parts. Also, signals for the –Fe–O bond at 618 cm^{-1} and for the -OH group at 3410 cm^{-1} are observed.

SEM and TEM techniques were applied to study the microstructure of the synthesized NPs (Fig. 3a–c) and demonstrated the synthesis of nano-sized particles with spherical shapes. TEM image (Fig. 3b) represents the generation of core/shell particles and emphasizes forming the Fe_3O_4 layer over the nZVI core. Figure 3a shows that NPs are in the size range of less than 30 nm. Also, the SEM image of nZVI@Fe_3O_4@IL (Fig. 3c), represents the deposition of IL layers over the surface of synthesized NPs. The element distributions of N, Fe, C, O, F, and P for synthesized nZVI@Fe_3O_4@IL NPs were obtained using mapping analysis and

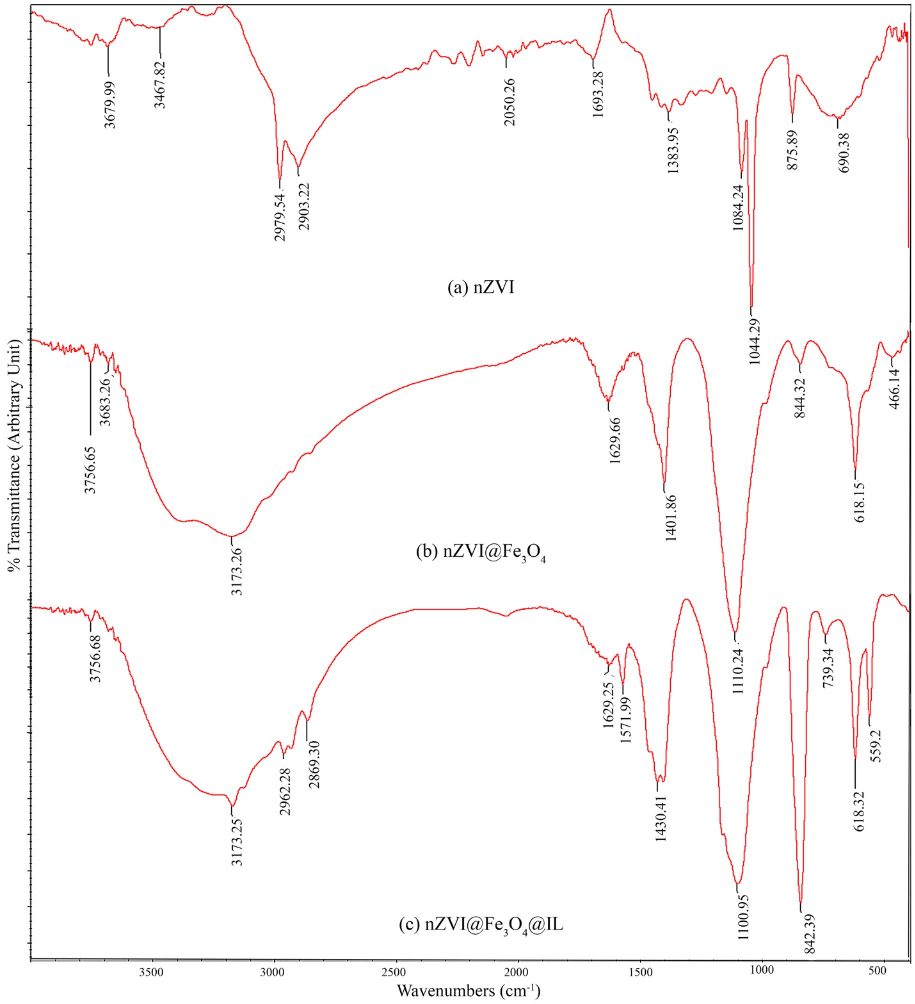

Fig. 2 FT-IR spectra of **a** nZVI, **b** nZVI@Fe_3O_4, and **c** nZVI@Fe_3O_4@IL

Fig. 3 **a**, **c** SEM image of nZVI@Fe_3O_4 and nZVI@Fe_3O_4@IL, **b** TEM image of nZVI@Fe_3O_4, **d** EDX mapping of nZVI@Fe_3O_4@IL, **e** XRD pattern for nZVI and nZVI@Fe_3O_4, **f** The VSM of nZVI@Fe_3O_4 and nZVI@Fe_3O_4@IL, **g** pH_{final} vs. $pH_{initial}$ Curve for determination of pH_{pzc}

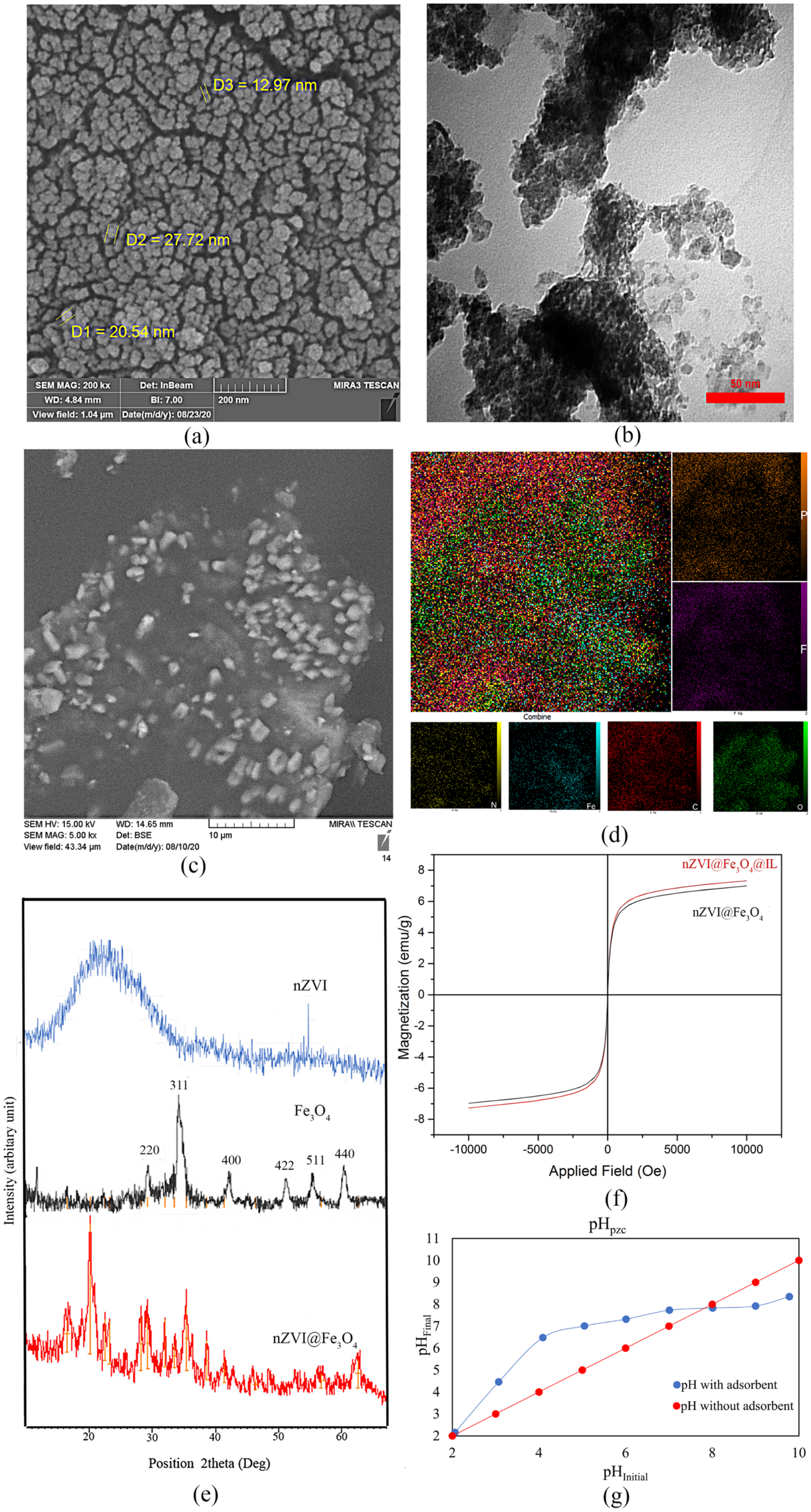

are presented in Fig. 3d, which emphasizes the coverage of ILs over the NPs surface.

The XRD pattern of nZVI@Fe_3O_4 NPs was compared with the patterns of Fe_3O_4 (Huang et al. 2015) (Fig. 3e). The sharp diffraction peak with 2θ at 22° and 32°, 36° match with polyphenols and Fe_3O_4 patterns, respectively (Loh et al. 2008). Observation of iron oxides and iron oxyhydroxides instead of Fe^0 can be related to the amorphous nature of synthesized Fe particles using tea extracts (Shahwan et al. 2011). Also, peaks with 2θ at 26°, 42°, 53° and 57° indicates the crystalline cubic structure of the synthesized NPs (Toutounchi et al. 2021).

The magnetic properties of the synthesized NPs were characterized by a VSM instrument (Fig. 3f). The saturation magnetization values of nZVI@Fe_3O_4 and nZVI@Fe_3O_4@IL were 6.5 and 6.7 emu g^{-1}, respectively, which indicates a suitable magnetic response of the synthesized NPs to the magnetic fields and confirms their superparamagnetic behavior. The partially increased value of saturation magnetization of nZVI@Fe_3O_4@IL compared to nZVI@Fe_3O_4, can be ascribed to the agglomeration of the NPs during surface coating with IL.

Physisorption hysteresis is a fundamental method for the characterization of pore structure. In this work, N_2 sorption measurements at 77 K were used for nZVI@Fe_3O_4 NPs (Fig. 4a–d). The obtained results were fit with the type IVa curve of IUPAC classification of physisorption isotherms (Lowell et al. 2012). Also, hysteresis loops

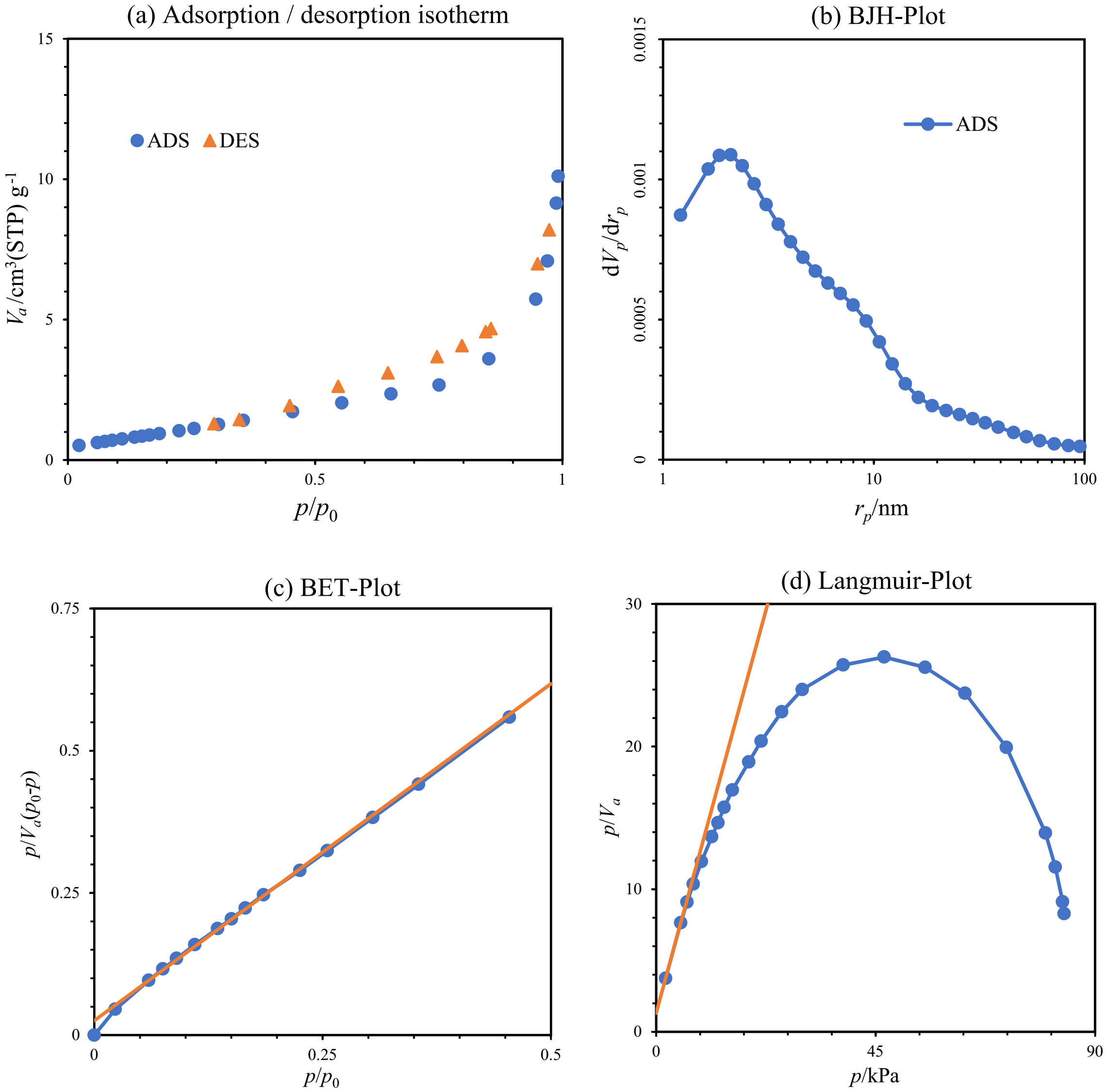

Fig. 4 The pore size distribution curves **a** N_2 adsorption/desorption isotherms, **b** BJH-plot, **c** Brunauer–Emmett–Teller (BET) plot, **d** Langmuir-plot

of magnetic NPs were matched with the H_3 type of IUPAC classification (Sing and Williams 2004).

The pore size distribution was calculated by the BJH formula (Fig. 4b). Values for V_p (the mean volume of the pores), a_p (surface of pores), and $r_{p,\,\mathrm{Peak\ (area)}}$ were obtained as 0.015281 $cm^3\ g^{-1}$, 4.6718 $m^2\ g^{-1}$, and 1.85 nm, respectively.

The surface area of magnetic NPs was measured by the BET method. Equation (2) expresses the linear form of the BET model:

$$\frac{\frac{p}{p^0}}{V_a\left(1-\frac{p}{p^0}\right)}=\frac{1}{V_mC}+\frac{C-1}{V_mC}\left(\frac{p}{p^0}\right), \qquad (2)$$

where V_a and V_m are the specific amounts adsorbed at the corresponding pressure p/p^0 and BET monolayer capacity, respectively. Also, the value of C provides a practical demonstration of the type of isotherm in the BET range, which is exponentially correlated with the energy of monolayer adsorption.

BET plot (Fig. 4c, R^2 = 0.9978) was applied to estimate the BET surface area. According to this procedure, the values of $a_{s,\,\mathrm{BET}}$ (specific BET surface area) = 3.5975m^2g^{-1}, V_m (BET monolayer capacity) = 0.8265 cm^3(STP) g^{-1}, C = 47.378, total pore volume ($\frac{p}{p^0}$= 0.990) = 0.14998 cm^3g^{-1} and mean pore diameter =16.68 nm were obtained.

Also, the specific surface area of NPs was calculated by the Langmuir isotherm. The curve of the Langmuir isotherm (Fig. 4d) showed that $a_{s,\,\mathrm{Lang}}$= 3.4662 m^2g^{-1} and V_m =0.7964 cm^3(STP)g^{-1}.

Experimental Design: Statistical Analysis of Data

The results of the suggested experiments by Taguchi OA_{16} design (Table 1) were analyzed using Minitab® 18 software. The mean values for the four levels of each parameter displayed how the Cr (VI) removal efficiencies change with the variation of the level of each factor (Fig. 5).

The electrostatic interaction between the Cr (VI) ions and the surface of NPs is significantly affected by the solution pH. Different species of Cr (VI) including H_2CrO_4, $HCrO_4^-$, CrO_4^{2-} and $H_2Cr_2O_7$ are in equilibrium in aqueous solutions. Due to the pK_a values of chromate acid–base couple ($pK_{a1\ H2CrO4/HCrO4^-}=0.75$, $pK_{a2\ HCrO4^-/CrO4^-}=6.4$), it is predicted to have $HCrO_4^-$ as dominant species of Cr (VI) at pH < 5, whereas at pH > pK_{a2}, the CrO_4^{2-} ions are the predominant species of Cr (VI) (Sanchez-Hachair and Hafmann 2018). The effect of solution pH on the removal efficiency was observed for different pH values (2, 3.5, 5, 7) at a constant CrO_4^{2-} ion initial concentration (40 mg L^{-1}) and a sample volume of 25 mL. It was found that the adsorption capacity was decreased noticeably from 84 to 52%, while the pH value raised from 2.0 to 7.0 (Fig. 5a). This observation can be ascribed to the positively charged surface of the nZVI@Fe_3O_4@IL NPs. The results showed pH_{pzc} = 7.8, demonstrates at pH_s<pH_{pzc}, the surface of NPs has a positive charge. So, Cr (VI) ions were adsorbed effectively as $HCrO_4^-$ through electrostatic interactions at pH = 2. For pH_s > 3.5, the removal efficiency of Cr (VI) ions was decreased dramatically due to reducing the positive sites on the adsorbent surface and subsequently, decrease in the electrostatic interaction between the adsorbent/adsorbate. So, pH = 2 was selected as the optimum value.

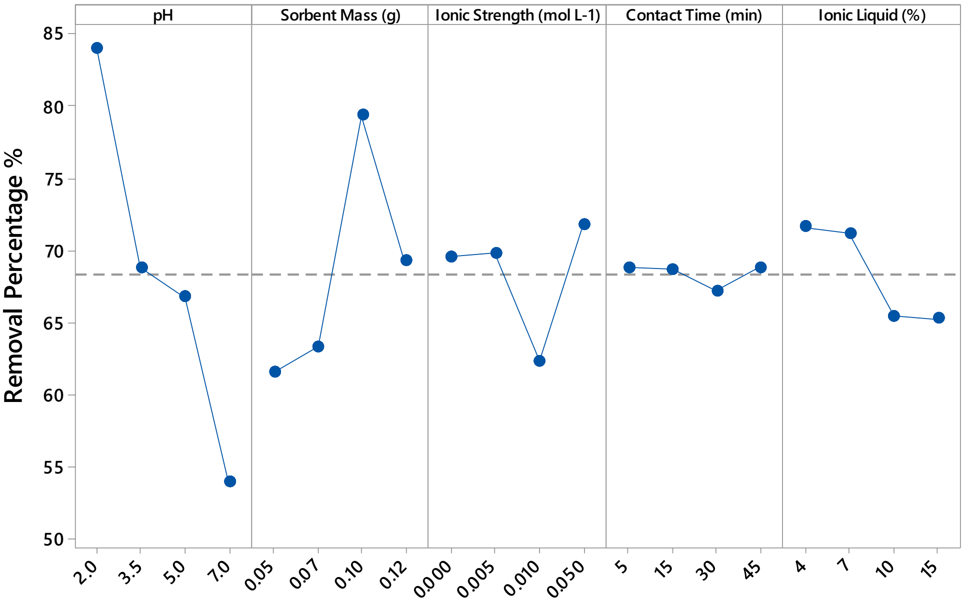

Fig. 5 The effect of **a** pH, **b** sorbent mass, **c** ionic strength, **d** contact time, and **e** ionic liquid on the Cr (VI) removal efficiency (sample volume: 25 mL, $C_{CrO_4^{2-}}$ = 40 mg L^{-1})

The sorbent mass contribution on the Cr (VI) removal efficiency was evaluated with sorbent masses of 0.05 0.07, 0.1, and 0.12 g. According to the results, the Cr (VI) removal efficiency enhances with increasing the adsorbent dosage and reaches its highest value at 80% for 0.1 g of the adsorbent (Fig. 5b). However, a further increase of adsorbent mass decreases Cr (VI) removal efficiency. This observation can be ascribed to the aggregation of NPs, which decreases the total surface area of the NPs. So, 0.1 g (2.5 g L^{-1}) for 25 mL CrO_4^{2-} solutions (40 mg L^{-1}) was considered as the optimum dose of the nZVI@Fe_3O_4@IL NPs.

The effect of salt on the Cr (VI) removal was evaluated by adjusting the salinity of sample solutions with different concentrations of NaCl solutions (0, 0.005, 0.01 and 0.05 M). It was highlighted that the removal efficiency improved by increasing the NaCl concentration (Fig. 5c). These results can be related to the effect of ionic strength on the interface potential and on the double layer thickness that affect the attachment of the adsorbed ions (Adegoke et al. 2014). Thus, further studies were conducted with adjusting the ionic strength with NaCl at 0.05 M.

The effect of different contact times (5–45 min) on the Cr (VI) adsorption efficiency using the nZVI@Fe_3O_4@IL NPs is shown in Fig. 5d. According to the results, there is no significant difference in removal efficiencies during the first 15 min of adsorption process and after that the removal efficiency is decreased up to 30 min. It can be concluded that all active sites of the NPs are available for Cr (VI) adsorption in early moments. Due to this result, further experiments were done at 10 min of contact time.

To investigate the effect of HMIMPF6 concentration on the Cr (VI) removal efficiency, four different IL solutions were prepared in chloroform (4, 7, 10, and 15% *v*/*v*). At higher IL concentrations, a reduction in the removal efficiency was observed (Fig. 5e) due to the decrease in the number of active sites resulting from the agglomeration of NPs. So, for the maximum adsorption, the subsequent experiments were done with coating of the nZVI@Fe_3O_4 NPs with a 4% IL solution.

The analysis of variance (ANOVA) is a set of statistical models and can be applied for evaluating the OA_{16} experiment results. The ANOVA results (Table 2) for the mean of responses from 32 experiments (2 repeats of 16 experiments) revealed that the pH amount is the main affecting parameter on the Cr (VI) adsorption efficiency with the highest percent contribution (57.56%). The following important parameters are sorbent mass (12.21%) and after that IL concentration (3.93%), ionic strength (1.17%) and contact time (< 1%), respectively.

Study of Adsorption Kinetics

The adsorption kinetic is known as a key factor for selecting the best possible adsorbent/adsorbate system and is essential to compare the results of various experimental conditions to the predicted adsorption parameters assessed by models and present considerable data that can be applied to design adsorption processes (Largitte and Pasquier 2016; Esmaeeli et al. 2017). To determine the kinetic parameters, the adsorption capability of Cr (VI) ions was considered at two concentrations of 40 and 100 mg L^{-1} in the various contact time (0–90 min) (sample volume = 25 mL, adsorbent dosage = 0.1 g, solution pH = 2, ionic strength = 0.05 mol L^{-1} and ionic liquid = 4% *v*/*v*). The mathematical equations relating to the pseudo-first order, pseudo-second order, intraparticle diffusion, and Elovich kinetic models were applied to investigate the adsorption kinetics of Cr (VI). The linear forms of kinetic models, along with the definitions of each parameter, are listed in Table 3. The slope and intercept of the linear plot of each model were used to calculate the values of Cr (VI) adsorption onto the nZVI@Fe_3O_4@IL parameters at two different concentrations (40 and 100 mg L^{-1}). The pseudo-first order kinetic model developed by Lagergren (Freundlich 1906) is a known model for the kinetic study of the water pollutants and considers a linear correlation between log (q_e–q_t) and time. Using this model, the rate constant (k_1, min^{-1}) and the equilibrium adsorption capacity (q_e, mg g^{-1}) are calculated from the slope and intercept of

Table 2 ANOVA results for Cr (VI) adsorption onto nZVI@Fe_3O_4@IL

Source	DF[a]	SS[b]	MS[c]	*F* value	*p* value	PC[d] (%)
pH	3	1695.9	565.3	12.22	0.000207	57.56
Sorbent mass	3	359.8	119.933	2.59	0.088885	12.21
Ionic strength	3	34.452	11.484	0.24	0.867157	1.17
Contact time	3	0.35398	0.1179	0.0025	0.99982	0.01
Ionic liquid	3	115.66	38.553	0.83	0.496641	3.93
Error	16	740.03	46.251			25.12

[a] Degrees of freedom

[b] Sum ofsquares

[c] Mean of squares

[d] Percentage of contribution

Table 3 Parameters of kinetic models for Cr (VI) (as $CrO_4{}^{2-}$) removal by the nZVI@Fe_3O_4@IL NPs

Kinetic models	Linear form equation	Results	
		40 mg L^{-1}	100 mg L^{-1}
Pseudo-first order	$\ln(q_e - q_t) = \ln(q_e) - k_1 t$	$q_{e,\text{cal}}$ = 1.004 mg g^{-1} k_1 = −0.0336 min^{-1} R^2= 0.9157	$q_{e,\text{cal}}$= 1.2832 mg g^{-1} k_1= 0.0193 min^{-1} R^2=0.9626
Pseudo-second order	$\frac{t}{q_t} = \frac{1}{k_2 q_e^2} + \left(\frac{1}{q_e}\right)t$	$q_{e,\text{cal}}$ = 9.2336 mg g^{-1} k_2= 0.4203 g mg^{-1} min^{-1} R^2 = 1	$q_{e,\text{cal}}$ = 21.4592 mg g^{-1} k_2=0.1497 g mg^{-1} min^{-1} R^2 = 1
Intraparticle diffusion	$q_t = k_p t^{1/2} + C$	C_0= 8.2367 mg g^{-1} k_p= 0.1318 mg g^{-1} $min^{-1/2}$ R^2= 0.6866	C_0= 20.755 mg g^{-1} k_p= 0.1935 mg g^{-1} $min^{-1/2}$ R^2= 0.8566
Elovich	$q_t = \frac{1}{\beta}\ln(\alpha\beta) + \frac{1}{\beta}\ln(t)$	α: 8.83*e*+12 (mg g^{-1} min^{-1}) β: 3.8022 (g mg^{-1}) R^2= 0.9293	α: 5.63e+24 (mg g^{-1} min^{-1}) β: 2.7956 (g mg^{-1}) R^2= 0.9949

Models Description: Pseudo-first order: q_e the dose of $CrO_4{}^{2-}$ adsorbed at equilibrium (mg g^{-1}), q_t the dose of $CrO_4{}^{2-}$ adsorbed at t (mg g^{-1}), k_1 pseudo-first-order rate constant (min^{-1}), Pseudo-second order: k_2 pseudo-second-order rate constant (g mg^{-1} min^{-1}), intraparticle diffusion: k_p rate constant of the intraparticle diffusion (mg g^{-1} $min^{-1/2}$), Elovich: α initial rate of adsorption (mg g^{-1} min^{-1}), β the extent of surface coverage and activation energy for chemisorption (g mg^{-1})

the plot. The pseudo-second order kinetic model assumes the sorption process is controlled by chemical processes. The plot of t/q_t vs the adsorption time (t) is linear from which k_2 and q_e can be obtained. Based on this model, the adsorption capacity directly relates to the adsorbent active sites occupied on the adsorbent (Ho and McKay 1999). The chemisorption involves exchanging, transferring, or sharing electrons among the adsorbate/adsorbent system (Ahmad et al. 2012). According to this model, although in the initial stages, due to the free adsorption surfaces, adsorption on the adsorbent is rapid, with the advancement of the adsorption process, the adsorption rate decreases by more occupation of active sites of the adsorbent.

The intraparticle diffusion model considers the sorption process either dominated by the mass transfer in the liquid phase or intraparticle mass transfer. This model investigates the adsorption process via a mechanistic perspective and presumes the intraparticle diffusion as the rate-controlling step (Öztürk and Malkoc 2014) and the solute uptake value alteration is in almost direct relation with the square root of time. In this model, a linear correlation from the plot of q_t versus $t^{1/2}$ (known as Weber-Morris plot) means the sorption process is dominated by intraparticle diffusion (Weber and Morris 1963). However, if the data exhibit multi-linear plots, then, two or more rate limiting steps influence the sorption process. It assumes that the external resistance to mass transfer to the adsorbent is significant only in the first section of plot that have more slope. The second linear portion is the gradual adsorption stage with controlling intraparticle diffusion (Fierro et al. 2008). According to Fig. 6c, the first and second straight lines representing macropore/mesopore, and micropore diffusion, respectively (Allen et al. 1989). Extrapolation of the linear portions of the plots back to the q_t values gives the intercepts (C), which provide the measure of the boundary layer thickness. The larger C value shows the boundary layer effect is greater.

The Elovich model, which is based on the adsorption capacity of the adsorbent, is more appropriate for chemical adsorption and systems with heterogeneous surfaces. If this model is feasible and the adsorption process fits this model, plotting q_t against ln (t) creates a linear relationship with a slope of $1/\beta$ and intercept of $1/\beta \ln(\alpha\beta)$.

The pseudo-second order displayed the best fit to data regarding the high correlation coefficient ($R^2 = 1$, Fig. 6b). Following this model, with increasing the initial concentrations of Cr (VI) (as $CrO_4{}^{2-}$ ion) from 40 to 100 mg L^{-1}, the k_2 value (g mg^{-1} min^{-1}) decreases (from 0.4212 to 0.1497 g mg^{-1} min^{-1}). Furthermore, $q_{e,\text{cal}}$ (mg g^{-1}) value is in direct correlation with Cr (VI) concentration variations (increases from 9.23 to 21.46 mg g^{-1}). This result indicates that the chemical processes control the overall rate of the adsorption process.

Figure 7 shows the initial UV–Vis absorption spectrum for 100 mg L^{-1} $CrO_4{}^{2-}$ ions before the adsorption process and after adsorption at various contact times. The spectra confirm the significant removal of Cr (VI) ions from the solution.

Study of Adsorption Isotherms

Adsorption equilibrium data are the most important part of information needed for a proper understanding of an adsorption process. These data are essential for developing pathways for adsorption mechanisms and designing efficient

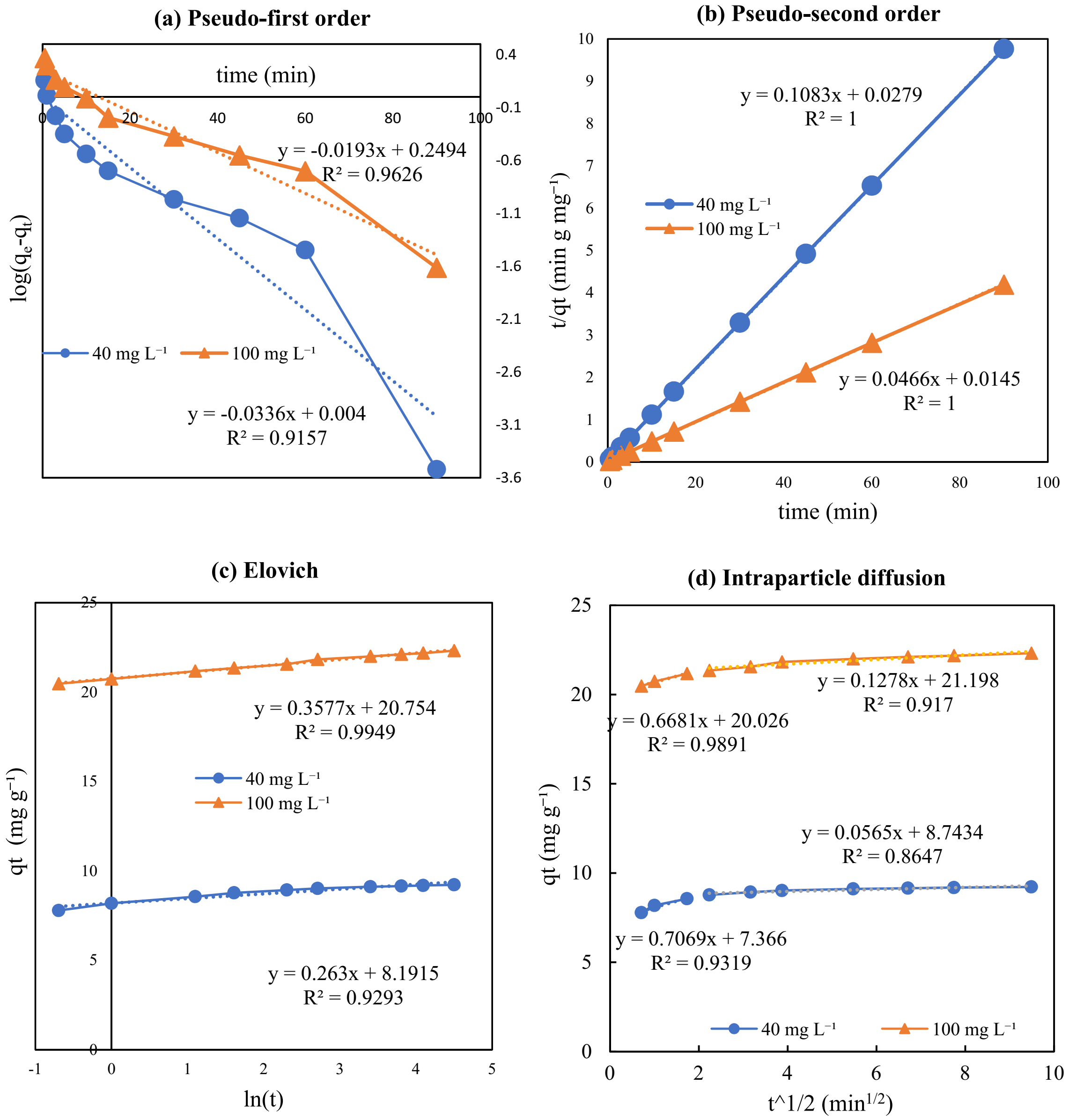

Fig. 6 **a** Pseudo-first order, **b** Pseudo-second order, **c** Intraparticle diffusion, **d** Elovich kinetics plot of Cr (VI) sorption onto synthesized NPs (sample volume = 25 mL, adsorbent dosage = 0.1 g, solution pH = 2, ionic strength = 0.05 mol L^{-1}, ionic liquid = 4% *v*/*v*, $C_{CrO_4^{2-}}$ = 40 and 100 mg L^{-1})

adsorption systems (Ayawei et al. 2017). Langmuir, Freundlich, Temkin, and Dubinin-Radushkevich's two-parameter isotherm models are frequently used to explain the interaction between the adsorbate and adsorbent at equilibrium. A proper understanding and interpretation of adsorption isotherms are critical for the overall improvement of adsorption mechanism pathways and effective design of adsorption systems. The adsorption isotherms of Cr (VI) ions on the nZVI@Fe_3O_4@IL NPs were investigated in different concentrations of CrO_4^{2-} ions (5–250 mg L^{-1}) by adding 0.1 g of the synthesized NPs at pH2 and ionic strength = 0.05 mol L^{-1} (at r.t). In addition to the previously mentioned two-parameter models, three-parameter models (Redlich-Peterson, Sips, and Toth) were also studied.

Langmuir isotherm is applied for quantification of the adsorptive capacity of different adsorbents (Mittal et al. 2007). This isotherm model has four primary presumptions (Kecili and Hussain 2018): (a) The adsorbent surface contains the adsorbing sites where adsorption occurs, (b) all sites are identical and have equal energy of adsorption, (c) the surface of the adsorbent is covered with a monolayer of adsorbed molecules (d) there is no interaction between adjacent adsorbed molecules on the adsorbent surface.

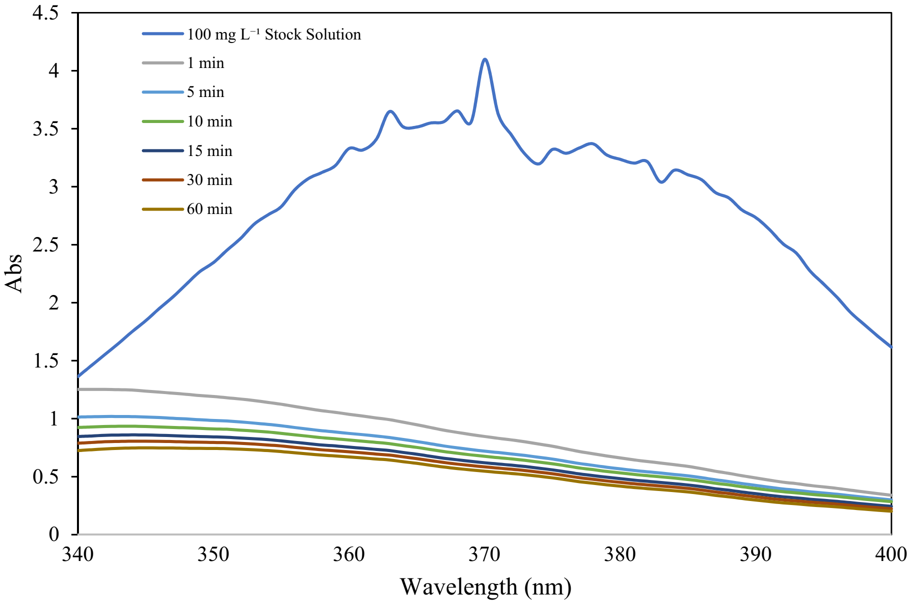

Fig. 7 UV–Vis absorption spectrum of CrO_4^{2-} for 100 mg L^{-1} stock solution and after adsorption onto the nZVI@Fe_3O_4@IL NPs during 1–60 min adsorption process (sample volume = 25 mL, adsorbent dosage = 0.1 g, solution pH = 2, ionic strength = 0.05 mol L^{-1}, ionic liquid = 4% *v*/*v*)

The linear form of the Langmuir equation is as follows (Eq. 3) (Dąbrowski 2001):

$$\frac{C_e}{q_e} = \frac{1}{q_m K_l} + \frac{C_e}{q_m}, \tag{3}$$

where C_e is the concentration of the Cr (VI) (as mg L^{-1} CrO_4^{2-} ion) at equilibrium, q_e is the equilibrium adsorption capacity (mg g^{-1}), K_1 is the constant associated with the free energy of adsorption (L mg^{-1}), and q_m is the maximum adsorption capacity at monolayer coverage (mg g^{-1}).

Freundlich isotherm model is utilized to study adsorption phenomena on heterogonous surfaces (Ayawei et al. 2015). Although, the Freundlich equation provides important information regarding the adsorption of particles, it has the following limitations (Singh 2016): (a) the Freundlich equation is entirely empirical, (b) the equation is valid only for a limited range of concentrations, (c) the constant K is temperature-dependent.

The linear form of the Freundlich model is as follows (Eq. 4) (Boparai et al. 2011):

$$\ln q_e = \ln K_f + \frac{1}{n} \ln \mathrm{C}_e, \tag{4}$$

where K_f (mg^{1+n} g^{-1} L^n) indicates the adsorption capacity, and *n* is the adsorption intensity. The value of 1/*n* lower than 1 represents a normal Freundlich isotherm, while cooperative adsorption has larger values.

Temkin isotherm is applied to investigate the role of indirect adsorbate/adsorbate interactions in an adsorption process. By ignoring the extremely low and large values of concentrations, it is also assumed that the heat of adsorption of all molecules in the layer decreases linearly as a result of increased surface coverage (Shariati et al. 2020). The following equation gives the Temkin isotherm linear form (Eq. 6) (Vijayaraghavan et al. 2006):

$$B = \frac{\mathrm{RT}}{b}, \tag{5}$$

$$q_e = B \ln A + B \ln C_e, \tag{6}$$

where *A*, *b*, and *B* represent the Temkin isotherm equilibrium binding constant (L g^{-1}), the constant associated with the heat of sorption (j mol^{-1}) and Temkin isotherm constant, respectively.

Dubinin-Radushkevich isotherm is an empirical adsorption model. It is usually applicable to express the adsorption mechanism with Gaussian energy distribution onto heterogeneous surfaces (Celebi et al. 2007). It is temperature-dependent; hence, all suitable data can be obtained by plotting adsorption data as a function of the ln(q_e) against ε^2 at various temperatures (Günay et al. 2007).

Dubinin-Radushkevich isotherm is represented as follows (Eqs. 7, 8) (Ayawei et al. 2015):

$$\ln q_e = \ln q_m - \beta\varepsilon^2, \tag{7}$$

$$\varepsilon = \mathrm{RT} \ln\left(1 + \frac{1}{C_e}\right), \tag{8}$$

where ε, β, *R*, and *T* represent Polanyi potential, Dubinin-Radushkevich constant (mol^2 K^{-1} J^{-2}), universal gas constant (8.31 $Jmol^{-1}$ k^{-1}), and absolute temperature, respectively.

The Redlich-Peterson (RP) isotherm model is a hybrid isotherm that presents both Langmuir and Freundlich isotherms in a single equation (Redlich and Peterson 1959). It is more accurate than those two models by incorporating three parameters into an empirical equation. The RP isotherm is expressed as follows (Eq. 9):

$$q_e = \frac{K_{\mathrm{RPC}} C_e}{1 + a_{\mathrm{RP}} C_e^{\beta_{\mathrm{RP}}}}, \tag{9}$$

where K_{RP} is RP model constant (L g^{-1}), a_{RP} is the affinity coefficient (Lmg^{-1}) and β_{RP} is the heterogeneity coefficient. The range for β_{RP} is from 0 to 1. For $\beta_{\mathrm{RP}} = 1$, the RP equation transform to the Langmuir model. Also, for K_{RP} and a_{RP} bigger than unity, the equation may transform to the Freundlich model (Lalhruaitluanga et al. 2010).

The Sips isotherm is applied for predicting the heterogeneous adsorption systems. This model resulted from the combination of Langmuir and Freundlich models to acquit their limitations and satisfying both low and high sorbate concentrations. It transforms to the Freundlich model for lower concentrations, and at the high-end boundary of concentrations performs like Langmuir. The non-linear Sips isotherm is as follows (Eq. 10):

$$q_e = \frac{Q_s K_S C_e^{1/n_S}}{1 + K_S C_e^{1/n_S}}, \tag{10}$$

where Q_S, K_S, and n_S represent the maximum adsorption capacity (mg g^{-1}), Sips constant (L g^{-1}), and the Sips dimensionless exponent, respectively. For $n_S = 1$, the equation converts to Langmuir form. While, as either K_S or C_e equals 0, Sips isotherm transform to Freundlich model (Belhachemi and Addoun 2011).

Toth isotherm model is also established to develop the Langmuir model and is suitable for heterogeneous adsorption systems studies. The non-linear and linear forms of Toth isotherm are expressed as Eqs. 11 and 12, respectively:

$$q_e = \frac{K_{\mathrm{T}} \mathrm{C}_e}{(a_T + C_e)^{1/t}}, \tag{11}$$

$$\ln\left(\frac{q_e}{K_T}\right) = \ln\left(C_e\right) - \frac{1}{t}\ln(a_T + C_e), \tag{12}$$

where K_T is Toth constant (mg g^{-1}), a_T is the affinity coefficient (L mg^{-1}) and t is the Toth exponent (dimensionless) and is associated with the surface heterogeneity. Toth exponent equals 1 for the process which occurs on a homogeneous surface (Brdar et al. 2012).

The values for all seven models are reported in Table 4. The Freundlich isotherm model shows better fitting rather than the other two-parameter models. The higher correlation coefficient ($R^2 = 0.9697$) of the Freundlich refers to the heterogeneity of the adsorbent sites. The Freundlich constant ($1/n$) was smaller than 1 due to high adsorption intensity and indicating the favorability of the adsorption. The maximum monolayer adsorption capacity (q_m) of Cr (VI) (as CrO_4^{2-} ions) onto the surface of nZVI@Fe_3O_4@IL NPs was obtained as 56.49 mg g^{-1} at 298 K.

MATLAB's fmincon function was used to compare the performance of two- and three- parameters isotherm models to minimize the mean squared error for q_e. The optimization algorithm was set to interior point. The reason for using fmincon is that it enables us to apply conditions to the unknown parameters of the model. For example, the exponent β_{RP} in the RP model lies between 0 and 1, and other parameters are non-negative. Furthermore, since raising a negative number to a real power might produce complex numbers, unconditional optimization for models such as the Toth isotherm could lead to problems, considering measurement error and the non-linear nature of the model. Other optimization options have been left on the default MATLAB settings.

By analyzing the results, we see that several and very different values for the parameters of the RP, Sips, and Toth models all give high R^2 and low root mean squared error (RMSE) values (Sips and Toth curves are overlapped in Fig. 8e), which indicates that these models are too powerful to model the measurements, and they are over-fitting to data. Since these models all have three parameters and are highly non-linear, they use their full potential to explain the variance in the data, ignoring the fact that part of this variance is due to measurement error. Non-linear regression can fit many more types of curves, but it can require more effort to present the best fit and interpret the role of the independent variables. Additionally, R^2 is not valid for non-linear regression (Spiess and Neumeyer 2010), and it is impractical to calculate p values for the parameter estimates. Considering the limitations of gathering more data which is inherent to such problems in chemistry, and since lower-dimensional models such as Langmuir and Freundlich isotherms appear to be performing well while having fewer parameters and non-linearity, there is little benefit in using more powerful and non-linear models such as Redlich-Peterson isotherm. Nevertheless, obtained values for K_{RP} (L g^{-1}) = 4.0208e + 06, K_s (L g^{-1}) = 4.1498e − 05, and $t = 3.1975$ confirms the transformation of all three-parameter models to the Freundlich model. Furthermore, close values for $n_s = 1.4515$ and $n_F = 1.5144$ of the Freundlich model confirm the Sips model has better agreement with the experimental data than the other three-parameters isotherm model (Table 4).

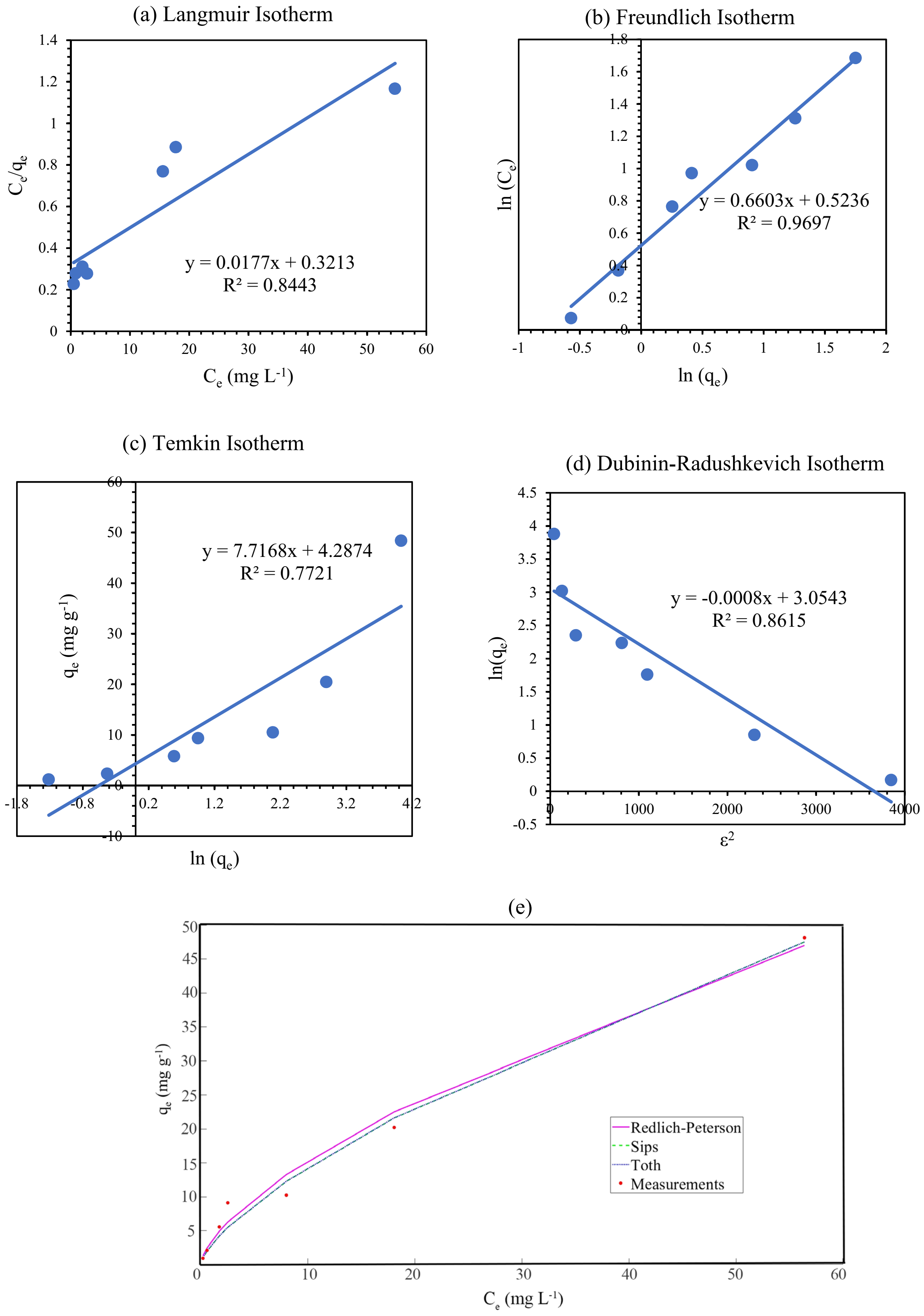

Fig. 8 **a** Langmuir, **b** Freundlich, **c** Temkin, **d** Dubinin-Radushkevich, **e** Redlich-Peterson, Sips, and Toth isotherm plots for adsorption of Cr (VI) onto the surface of nZVI@Fe$_3$O$_4$@IL NPs (sample volume = 25 mL, adsorbent dosage = 0.1 g, solution pH = 2, ionic strength = 0.05 mol L^{-1}, ionic liquid = 4% *v*/*v*, $C_{CrO_4^{2-}}$ = 5–250 mg L^{-1})

Table 4 Parameters of adsorption isotherms for Cr (VI) (as CrO_4^{2-}) removal by nZVI@Fe_3O_4@IL NPs

Isotherm model	Regression	Parameters
Langmuir	Linear	q_m(mg g^{-1}) = 56.49 K_l (L mg^{-1}) = 0.550 R^2 = 0.8443 RMSE = 3.0212
Freundlich	Linear	K_f(mg^{1+n} g^{-1} L^n) = 1.6880 n = 1.5144 R^2=0.9697 RMSE = 2.0673
Temkin	Linear	$b\left(\text{J mol}^{-1}\right)$ = 321.27 $A\left(\text{L g}^{-1}\right)$ =1.7428 R^2 = 0.7721 RMSE = 8.6084
Dubinin-Radushkevich	Linear	β (mol^2 K^{-1} J^{-2}) = 0.0008 E (kj mol^{-1}) = 0.025 R^2 = 0.8615 RMSE = 6.6817
Redlich–Peterson	Non-linear	K_{RP}(L g^{-1}) = 4.0208e + 06 a_{RP} (L mg^{-1}) = 1.1364e + 06 β_{RP} = 0.3574 R^2=0.9849 RMSE = 2.4750
Sips	Non-linear	Q_s (mg g^{-1}) = 7.1588e + 04 1/n_s = 0.6889 K_s (L g^{-1}) = 4.1498e – 05 R^2= 0.9868 RMSE = 2.3123
Toth	Non-linear	K_T(mg g^{-1}) = 2.9879 a_T (L mg^{-1}) = 3.5608e – 07 t = 3.1975 R^2= 0.9478 RMSE = 2.3113

Study of Adsorption Thermodynamics

To investigate the effect of temperature on the adsorption process, the thermodynamic parameters were estimated in the temperature range of 15–55 °C (288.15–328.15 K) at optimum condition ($C_{CrO4}{}^{2-}$ = 40 mg L^{-1}, sample volume = 25 mL, adsorbent mass = 0.1 g, solution pH = 2, ionic strength = 0.05 mol L^{-1}, contact time = 10 min, ionic liquid = 4% *v*/*v*). The Gibbs free energy change ($\Delta G°$) values can guess the spontaneous or nonspontaneous nature of the process. The negative values of $\Delta G°$ reveal a spontaneous process (Liu et al. 2010). The enthalpy change ($\Delta H°$) distinguishes between physical and chemical adsorption and also endothermic and exothermic processes. For endothermic processes, it has a positive value and it is negative for exothermic processes (Kumar et al. 2007). The entropy change ($\Delta S°$) predicts the magnitude of changes in the adsorbent surface (Ahmaruzzaman and Sharma 2005).

The Gibbs energy, $\Delta G°$ (kJ mol^{-1}), can be calculated from the Eqs. (13) and (14):

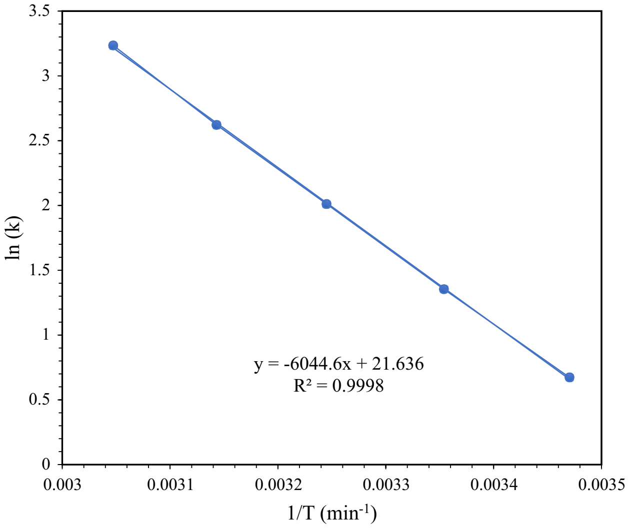

Fig. 9 The plot of ln *k* vs. 1/T. ($C_{CrO4}{}^{2-}$ = 40 mg L^{-1}, sample volume = 25 mL, adsorbent mass = 0.1 g, solution pH = 2, ionic strength = 0.05 mol L^{-1}, contact time = 10 min, ionic liquid = 4% *v*/*v*)

$$\Delta G° = \Delta H° = T\Delta S°, \tag{13}$$

$$\Delta G° = -\text{RT} \ln K, \tag{14}$$

K, the equilibrium constant, indicates the capability of the adsorbent to hold the adsorbate and measures the motion of the adsorbate within the solution (Lian et al. 2009).

The slope and intercept of a linear plot of ln *K* vs. 1/*T* give the values of $\Delta H°$ (kJ mol^{-1}) and $\Delta S°$ (J mol^{-1} K^{-1}) (Fig. 9).

The magnitude of $\Delta H°$ and $\Delta G°$ distinguish between physisorption and chemisorption. Generally, the $\Delta G°$ value is in the range of 0 to – 20 kJ mol^{-1} and – 80 to – 400 kJ mol^{-1} for physical and chemical adsorptions, respectively. The magnitude of the $\Delta H°$ value lies in the range of – 2.1 to – 20.9 and – 80 to – 200 kJ mol^{-1} for physical and chemical adsorptions, respectively. The magnitude and sign of $\Delta S°$ indicate whether the adsorption process is an associative or dissociative mechanism. A positive $\Delta S°$ value suggests the organization of the adsorbate at the solid/solution interface becomes more random, while negative value suggests the opposite fact. Table 5 represents the obtained thermodynamic parameters. It was found that the $\Delta G°$ is decreasing by raising the temperature from 15 to 55 °C. The $\Delta G°$ with negative values at several temperatures confirms the spontaneous nature of the process. The positive $\Delta H°$ (50.255 kJ mol^{-1}) reveals that the adsorption process is endothermic and more efficient at higher temperatures.

Removal of Cr (VI) Ions from Actual Samples

To investigate the potential of the nZVI@Fe_3O_4@IL NPs for Cr (VI) removal, the synthesized NPs were examined

Table 5 Thermodynamic parameters of Cr (VI) removal by nZVI@Fe_3O_4@IL NPs

$\Delta G°$ (kJ mol^{-1})					$\Delta H°$ (kJ mol^{-1})	$\Delta S°$ (kJ mol^{-1} K^{-1})
Temperature (K)					50.255	0.1799
288.15	298.15	308.15	318.15	328.15		
− 1.611	− 3.354	− 5.152	− 6.933	− 8.825		

on three real samples collected from the Caspian Sea, Rasht Well, and Tap Waters (Guilan, Iran). For this purpose, solutions of CrO_4^{2-} ions (40 mg L^{-1}) were prepared by spiking the real water samples, and the adsorption experiments were carried out under the optimized conditions (adsorbent mass: 0.1 g, pH 2, ionic strength 0.05 M, ionic liquid 4% and contact time 10 min). The removal efficiencies (%) were obtained as 89.9, 85.8, and 88.9 for the Caspian Sea, Well, and Tap waters, respectively. The result showed good removal efficiency of nZVI@Fe_3O_4@IL NPs for Cr (VI) ions in all of the samples and confirmed the capability of NPs for real samples.

Comparison with Other Adsorbents

Nowadays, the utilization of magnetite NPs to remove heavy metals is a prevalent and interesting subject. A comparison between the result of the current study and several other studies for removing Cr (VI) ions from aqueous solutions are listed in Table 6. Kim et al. (2012) investigated the adsorption performance of mesoporous iron nanocomposites for purifying chromate-contaminated wastewaters. Bishnoi et al. (2004) studied the application of activated rice husk for this purpose. The maximum removal of Cr (VI) (94.86%) was reported at pH 2 by activated rice husk, and adsorption followed the Freundlich isotherm. Aslani et al. (2018) studied the removal of Cr (VI) ions from water solution by a new magnetic polyhexamethylene biguanide modified chitosan NPs. The adsorption capacity of synthesized NPs was reported as 6.73 mg g^{-1} at pH 7. Daneshvar and Hosseini (2018) synthesized a cost-effective magnetic bio-adsorbent with maximum Cr (VI) removal of 92% at pH 5.8, adsorbent dose 3.72 g L^{-1}, Cr (VI) concentration 23.4 mg L^{-1}, and duration time 11 min. Samuel and coworkers (2018) developed a magnetic modified graphene oxide/chitosan/ferrite (GCF) nanocomposite to remove hexavalent chromium from aqueous solutions. The GCF displayed an adsorption capacity of 270.27 mg g^{-1} for Cr (VI) at pH 2. Fan and coworkers (2017) recycled tea waste by loading it with nano-Fe_3O_4 particles to prepare a magnetic tea waste/Fe_3O_4 (TW/Fe_3O_4) composite. The Langmuir isotherm model for chromium removal by TW/Fe_3O_4 displayed an adsorption capacity of 75.76 mg g^{-1}. Srivastava and Sharma (2013) synthesized and applied Fe_3O_4@n-SiO_2 NPs to remove hexavalent chromium from aqueous solutions. They reported that the optimum removal of Cr (VI) ions was achieved at a pH of 2.0 and the kinetic data followed the pseudo-second order model. Luo et al. (2013) developed a magnetic MnO_2/Fe_3O_4/o-MWCNTs nanocomposites and applied it for hexavalent chromium ion adsorption. Also, Luo conducted kinetic and thermodynamic studies. The pseudo-second order model properly described the data. The q_m was estimated to be 186.9 mg g^{-1} based on the Langmuir model. Hu et al. (2007) coated γ-Fe_2O_3 NPs with δ-FeOOH to improve hexavalent chromium removal. Equilibrium studies were conducted and the Langmuir isotherm model described Cr (VI) adsorption data excellently

Table 6 Comparison of the current study with some similar procedures for Cr (VI) (as $CrO_4^{\ 2-}$) removal

Adsorbents	q_m (mg g^{-1})	pH	Temperature (K)	Isotherm model	Kinetic model	References
Iron–iron oxide nanocomposites	34.1	7	293	Langmuir	Pseudo-first order	Kim et al. (2012)
Activated rice husk carbon	40	2	298	Freundlich		Bishnoi et al. (2004)
Magnetic Chitosan	6.73	7	298	Temkin	Pseudo-first order	Aslani et al. (2018)
Magnetic nanobiocomposite	14.64	5.8	313	Temkin	Pseudo-second order	Daneshvar and Hosseini (2018)
Graphene oxide/chitosan/ferrite nanocomposite	270.27	2	298	Langmuir	Pseudo-second order	Samuel et al. (2018)
Tea waste/Fe_3O_4	75.76	2	298	Langmuir	Pseudo-second order	Fan et al. (2017)
Fe_3O_4@n-SiO_2 NPs	3.78	2	298	Langmuir	Pseudo-second-order	Srivastava and Sharma (2013)
MnO_2/Fe_3O_4/o-MWCNTs	186.9	2	298	Langmuir	Pseudo-second-order	Luo et al. (2013)
Feroxyhyte-coated maghemite NPs	25.8	2.5	298	Langmuir	–	Hu et al. (2007)
Fe_3O_4@SiO_2@Kit-6	129.8	2	298	Langmuir	Pseudo-second-order	Shariati et al. (2017)
nZVI@Fe_3O_4@IL	**56.49**	2	**298**	**Freundlich**	**Pseudo-second-order**	**This work**

To show the bold row belongs to the present study and the q_m of the NPs, was estimated as 25.8 mg g^{-1}. The adsorption capacity of synthesized nZVI@Fe_3O_4@IL NPs shows better efficiency than some of the previously reported adsorbents as well as the proper magnetic properties.

Conclusion

The adsorption process has a significant role in water purification. The nZVI@Fe_3O_4@IL NPs were synthesized and applied for Cr (VI) removal from aqueous solutions. The proposed method utilizes both steel slag and *Camellia sinensis* extract for synthesizing magnetic NPs. As mentioned before, the combination of ILs and NPs provides electrostatic forces due to forming a cationic-anionic ion layer around the NPs.

The characterization methods confirmed the core/shell structure of synthesized NPs, including magnetic shell and IL layer over the NPs surface. The magnetic properties of NPs facilitate their application as adsorbents. nZVI@Fe_3O_4@IL NPs demonstrated impressive removal capabilities toward Cr (VI). The pseudo-second order kinetic model perfectly described the kinetic results. The kinetic study, showed the adsorption data obey from pseudo-second order kinetic model that indicates the chemical processes control the overall rate of the adsorption process. The study of effect of solution pH on the removal efficiency showed that Cr (VI) ions were adsorbed effectively through electrostatic interactions. Also, the results displayed that Freundlich isotherm is an appropriate model for equilibrium data. Owing to some significant properties such as good magnetic properties, short operation duration, user-friendliness, and proper removal efficiency in the real samples, the proposed NPs could be applicable for industrial purposes, including Cr (VI) removal from water and wastewaters.

Acknowledgements The authors are humbly thankful to Rasht Branch, Islamic Azad University, for supporting this study.

Declarations

Conflict of interests The authors declare that they have no known competing financial interests or personal relationships that could have appeared to influence the work reported in this paper.

References

Abbas A, Al-Amer AM, Laoui T, Al-Marri MJ, Nasser MS, Khraisheh M, Atieh MA (2016) Heavy metal removal from aqueous solution by advanced carbon nanotubes: critical review of adsorption applications. Sep Purif Technol 157:141–161. https://doi.org/10.1016/j.seppur.2015.11.039

Adegoke HI, AmooAdekola F, Fatoki OS, Ximba BJ (2014) Adsorption of Cr (VI) on synthetic hematite (α-Fe_2O_3) nanoparticles of different morphologies. Korean J Chem Eng 31(1):142–154. https://doi.org/10.1007/s11814-013-0204-7

Ahmad F, Daud WMAW, Ahmad MA, Radzi R (2012) Cocoa (theobroma cacao) shell-based activated carbon by CO_2 activation in removing of cationic dye from aqueous solution: kinetics and equilibrium studies. Chem Eng Res Des 90(10):1480–1490. https://doi.org/10.1016/j.cherd.2012.01.017

Ahmaruzzaman M, Sharma D (2005) Adsorption of phenols from wastewater. J Colloid Interface Sci 287(1):14–24. https://doi.org/10.1016/j.jcis.2005.01.075

Ali I, Gupta VK (2006) Advances in water treatment by adsorption technology. Nat Protoc 1(6):2661–2667. https://doi.org/10.1038/nprot.2006.370

Allen S, Mckay G, Khader K (1989) Intraparticle diffusion of a basic dye during adsorption onto sphagnum peat. Environ Pollut 56(1):39–50. https://doi.org/10.1016/0269-7491(89)90120-6

Aslani H, Kosari TE, Naseri S, Nabizadeh R, Khazaei M (2018) Hexavalent chromium removal from aqueous solution using functionalized chitosan as a novel nano-adsorbent: modeling and optimization, kinetic, isotherm, and thermodynamic studies, and toxicity testing. Environ Sci Pollut Res 25(20):20154–20168. https://doi.org/10.1007/s11356-018-2023-1

Ayawei N, Ekubo A, Wankasi D, Dikio E (2015) Adsorption of Congo Red by Ni/Al-CO_3: equilibrium, thermodynamic and kinetic studies. Open J Chem 31(3):1307–1318. https://doi.org/10.13005/ojc/310307

Ayawei N, Ebelegi AN, Wankasi D (2017) Modelling and interpretation of adsorption isotherms. J Chem 2017:3039817. https://doi.org/10.1155/2017/3039817

Barczak M, Michalak-Zwierz K, Gdula K, Tyszczuk-Rotko K, Dobrowolski R, Dąbrowski A (2015) Ordered mesoporous carbons as effective sorbents for removal of heavy metal ions. Microporous Mesoporous Mater 211:162–173. https://doi.org/10.1016/j.micromeso.2015.03.010

Belhachemi M, Addoun F (2011) Comparative adsorption isotherms and modeling of methylene blue onto activated carbons. Appl Water Sci 1(3–4):111–117. https://doi.org/10.1007/s13201-011-0014-1

Bishnoi NR, Bajaj M, Sharma N, Gupta A (2004) Adsorption of Cr (VI) on activated rice husk carbon and activated alumina. Bioresour Technol 91(3):305–307. https://doi.org/10.1016/S0960-8524(03)00204-9

Boparai HK, Joseph M, O'Carroll DM (2011) Kinetics and thermodynamics of cadmium ion removal by adsorption onto nano zerovalent iron particles. J Hazard Mater 186(1):458–465. https://doi.org/10.1016/j.jhazmat.2010.11.029

Brdar M, Šćiban M, Takači A, Došenović T (2012) Comparison of two and three parameters adsorption isotherm for cr(vi) onto kraft lignin. Chem Eng J 183:108–111. https://doi.org/10.1016/j.cej.2011.12.036

Celebi O, Üzüm Ç, Shahwan T, Erten HN (2007) A radiotracer study of the adsorption behavior of aqueous Ba^{2+} ions on nanoparticles of zero-valent iron. J Hazard Mater 148(3):761–767. https://doi.org/10.1016/j.jhazmat.2007.06.122

Chen H, Du P, Chen J, Hu S, Li S, Liu H (2010) Separation and preconcentration system based on ultrasonic probe-assisted ionic liquid dispersive liquid–liquid microextraction for determination trace amount of chromium (VI) by electrothermal atomic absorption spectrometry. Talanta 81(1):176–179. https://doi.org/10.1016/j.talanta.2009.11.054

Chen Y, Wang Q, Zhang Z, Tang J (2012) Determination of the solubility parameter of ionic liquid 1-hexyl-3-methylimidazolium hexafluorophosphate by inverse gas chromatography. Ind Eng Chem Res 51(46):15293–15298. https://doi.org/10.1021/ie301924y

Dąbrowski A (2001) Adsorption—from theory to practice. Adv Colloid Interface Sci 93(1):135–224. https://doi.org/10.1016/S0001-8686(00)00082-8

Dai W, Zheng M, Zhao Y, Liao S, Ji G, Cao J (2009) Template synthesis of three-dimensional cubic ordered mesoporous carbon with tunable pore sizes. Nanoscale Res Lett 5(1):103. https://doi.org/10.1007/s11671-009-9450-3

Danesh SMS, Faghihian H, Shariati S (2019) Sulfonic acid functionalized SBA-3 silica mesoporous magnetite nanocomposite for Safranin O dye removal. SILICON 11(4):1817–1827. https://doi.org/10.1007/s12633-018-9997-7

Daneshvar M, Hosseini MR (2018) Kinetics, isotherm, and optimization of the hexavalent chromium removal from aqueous solution by a magnetic nanobiosorbent. Environ Sci Pollut Res 25(28):28654–28666. https://doi.org/10.1007/s11356-018-2878-1

Daraei H, Mittal A, Mittal J, Kamali H (2014) Optimization of Cr (VI) removal onto biosorbent eggshell membrane: experimental and theoretical approaches. Desalin Water Treat 52(7–9):1307–1315. https://doi.org/10.1080/19443994.2013.787374

Du K, Li J, Bai Y, An M, Gao XM, Chang YX (2018) A green ionic liquid-based vortex-forced mspd method for the simultaneous determination of 5-hmf and iridoid glycosides from fructus corni by ultra-high performance liquid chromatography. Food Chem 244:190–196. https://doi.org/10.1016/j.foodchem.2017.10.057

Esmaeeli F, Gorbanian SA, Moazezi N (2017) Removal of estradiol valerate and progesterone using powdered and granular activated carbon from aqueous solutions. Int J Environ Res 11:695–705. https://doi.org/10.1007/s41742-017-0060-0

Fan S, Wang Y, Li Y, Tang J, Wang Z, Tang J, Li X, Hu K (2017) Facile synthesis of tea waste/Fe_3O_4 nanoparticle composite for hexavalent chromium removal from aqueous solution. RSC Adv 7(13):7576–7590. https://doi.org/10.1039/C6RA27781K

Fazlzadeh M, Rahmani K, Zarei A, Abdoallahzadeh H, Nasiri F, Khosravi R (2017) A novel green synthesis of zero valent iron nanoparticles (nzvi) using three plant extracts and their efficient application for removal of cr (vi) from aqueous solutions. Adv Powder Technol 28(1):122–130. https://doi.org/10.1016/j.apt.2016.09.003

Fierro V, Torné-Fernández V, Montané D, Celzard A (2008) Adsorption of phenol onto activated carbons having different textural and surface properties. Microporous Mesoporous Mater 111(1–3):276–284. https://doi.org/10.1016/j.micromeso.2007.08.002

Freundlich HM (1906) Over the adsorption in solution. J Phys Chem 57(1):385–471

Fukushima T, Aida T (2007) Ionic liquids for soft functional materials with carbon nanotubes. Chem Eur J 13(18):5048–5058. https://doi.org/10.1002/chem.200700554

Gong J, Liu T, Wang X, Hu X, Zhang L (2011) Efficient removal of heavy metal ions from aqueous systems with the assembly of anisotropic layered double hydroxide nanocrystals@ carbon nanosphere. Environ Sci Technol 45(14):6181–6187. https://doi.org/10.1021/es200668q

Gu S, Kang X, Wang L, Lichtfouse E, Wang C (2019) Clay mineral adsorbents for heavy metal removal from wastewater: a review. Environ Chem Lett 17(2):629–654. https://doi.org/10.1007/s10311-018-0813-9

Günay A, Arslankaya E, Tosun I (2007) Lead removal from aqueous solution by natural and pretreated clinoptilolite: adsorption equilibrium and kinetics. J Hazard Mater 146(1–2):362–371. https://doi.org/10.1016/j.jhazmat.2006.12.034

He Z, Alexandridis P (2017) Ionic liquid and nanoparticle hybrid systems: emerging applications. Adv Colloid Interface Sci 244:54–70. https://doi.org/10.1016/j.cis.2016.08.004

Ho Y-S, McKay G (1999) Pseudo-second order model for sorption processes. Process Biochem 34(5):451–465. https://doi.org/10.1016/S0032-9592(98)00112-5

Hu J, Lo IM, Chen G (2007) Performance and mechanism of chromate (VI) adsorption by δ-FeOOH-coated maghemite (γ-Fe_2O_3) nanoparticles. Sep Purif Technol 58(1):76–82. https://doi.org/10.1016/j.seppur.2007.07.023

Hua M, Zhang S, Pan B, Zhang W, Lv L, Zhang QJJOHM (2012) Heavy metal removal from water/wastewater by nano-sized metal oxides: a review. J Hazard Mater 211:317–331. https://doi.org/10.1016/j.jhazmat.2011.10.016

Huang L, Luo F, Chen Z, Megharaj M, Naidu R (2015) Green synthesized conditions impacting on the reactivity of fe nps for the degradation of malachite green. Spectrochim Acta A Mol Biomol Spect 137:154–159. https://doi.org/10.1016/j.saa.2014.08.116

Huang R, He L, Zhang T, Li D, Tang P, Feng Y (2018) Novel carbon paper@magnesium silicate composite porous films: Design, fabrication, and adsorption behavior for heavy metal ions in aqueous solution. ACS Appl Mater Interfaces 10(26):22776–22785. https://doi.org/10.1021/acsami.8b01557

Jamei MR, Khosravi MR, Anvaripour B (2014) A novel ultrasound assisted method in synthesis of nZVI particles. Ultrason Sonochem 21(1):226–233. https://doi.org/10.1016/j.ultsonch.2013.04.015

Karnib M, Kabbani A, Holail H, Olama Z (2014) Heavy metals removal using activated carbon, silica and silica activated carbon composite. Energy Procedia 50:113–120. https://doi.org/10.1016/j.egypro.2014.06.014

Kecili R, Hussain CM (2018) Chapter 4—mechanism of adsorption on nanomaterials. In: Hussain CM (ed) Nanomaterials in chromatography. Elsevier, Ney York, pp 89–115

Khabazipour M, Shariati S, Safa F (2016) SBA and kit-6 mesoporous silica magnetite nanoparticles: synthesis and characterization. Synth React Inorg Met Org Chem 46(5):759–765. https://doi.org/10.1080/15533174.2014.989583

Kim J-H, Kim J-H, Bokare V, Kim E-J, Chang Y-Y, Chang Y-S (2012) Enhanced removal of chromate from aqueous solution by sequential adsorption–reduction on mesoporous iron–iron oxide nanocomposites. J Nanopart Res 14(8):1010. https://doi.org/10.1007/s11051-012-1010-6

Kumar A, Kumar S, Kumar S, Gupta DV (2007) Adsorption of phenol and 4-nitrophenol on granular activated carbon in basal salt medium: equilibrium and kinetics. J Hazard Mater 147(1–2):155–166. https://doi.org/10.1016/j.jhazmat.2006.12.062

Lalhruaitluanga H, Jayaram K, Prasad M, Kumar K (2010) Lead (II) adsorption from aqueous solutions by raw and activated charcoals of melocanna baccifera roxburgh (bamboo)—a comparative study. J Hazard Mater 175(1–3):311–318. https://doi.org/10.1016/j.jhazmat.2009.10.005

Largitte L, Pasquier R (2016) A review of the kinetics adsorption models and their application to the adsorption of lead by an activated carbon. Chem Eng Res Des 109:495–504. https://doi.org/10.1016/j.cherd.2016.02.006

Li DC, Jiang JG (2010) Optimization of the microwave-assisted extraction conditions of tea polyphenols from green tea. Int J Food Sci Nutr 61(8):837–845. https://doi.org/10.3109/09637486.2010.489508

Li S, Yan W, Zhang W-x (2009) Solvent-free production of nanoscale zero-valent iron (nZVI) with precision milling. Green Chem 11(10):1618–1626. https://doi.org/10.1039/B913056J

Lian L, Guo L, Guo C (2009) Adsorption of Congo Red from aqueous solutions onto ca-bentonite. J Hazard Mater 161(1):126–131. https://doi.org/10.1016/j.jhazmat.2008.03.063

Liu J-f, Zhao Z-s, Jiang G-b (2008) Coating Fe_3O_4 magnetic nanoparticles with humic acid for high efficient removal of heavy metals in water. Environ Sci Technol 42(18):6949–6954. https://doi.org/10.1021/es800924c

Liu Q-S, Zheng T, Wang P, Jiang J-P, Li N (2010) Adsorption isotherm, kinetic and mechanism studies of some substituted phenols on activated carbon fibers. Chem Eng J 157(2–3):348–356. https://doi.org/10.1016/j.cej.2009.11.013

Loh KS, Yook Heng L, Musa A, Salmah A, Ishak Z (2008) Use of Fe_3O_4 nanoparticles for enhancement of biosensor response to the herbicide 2,4-dichlorophenoxyacetic acid. Sensors 8:5775–5791. https://doi.org/10.3390/s8095775

Lowell S, Shields JE, Thomas MA, Thommes M (2012) Characterization of porous solids and powders: surface area, pore size and density. Springer Science & Business Media, New York

Luo C, Tian Z, Yang B, Zhang L, Yan S (2013) Manganese dioxide/iron oxide/acid oxidized multi-walled carbon nanotube magnetic nanocomposite for enhanced hexavalent chromium removal. Chem Eng J 234:256–265. https://doi.org/10.1016/j.cej.2013.08.084

Mitra S, Sarkar A, Sen S (2017) Removal of chromium from industrial effluents using nanotechnology: a review. Nanotechnol Env Eng 2(1):11. https://doi.org/10.1007/s41204-017-0022-y

Mittal A, Kurup L, Mittal J (2007) Freundlich and langmuir adsorption isotherms and kinetics for the removal of tartrazine from aqueous solutions using hen feathers. J Hazard Mater 146(1–2):243–248. https://doi.org/10.1016/j.jhazmat.2006.12.012

Mustafa G, Tahir H, Sultan M, Akhtar N (2013) Synthesis and characterization of cupric oxide (CuO) nanoparticles and their application for the removal of dyes. Afr J Biotechnol 12(47):6650–6660. https://doi.org/10.5897/AJB2013.13058

Nisticò R, Carlos L (2019) High yield of nano zero-valent iron (nZVI) from carbothermal synthesis using lignin-derived substances from municipal biowaste. J Anal Appl Pyrolysis 140:239–244. https://doi.org/10.1016/j.jaap.2019.03.022

Oliveira H (2012) Chromium as an environmental pollutant: insights on induced plant toxicity. J Bot 2012:8. https://doi.org/10.1155/2012/375843

Öztürk A, Malkoc E (2014) Adsorptive potential of cationic Basic Yellow 2 (BY2) dye onto natural untreated clay (nuc) from aqueous phase: mass transfer analysis, kinetic and equilibrium profile. Appl Surf Sci 299:105–115. https://doi.org/10.1016/j.apsusc.2014.01.193

Pashai Gatabi M, Milani Moghaddam H, Ghorbani M (2016) Point of zero charge of maghemite decorated multiwalled carbon nanotubes fabricated by chemical precipitation method. J Mol Liq 216:117–125. https://doi.org/10.1016/j.molliq.2015.12.087

Peng C, Meng H, Song S, Lu S, Lopez-Valdivieso A (2005) Elimination of Cr (VI) from electroplating wastewater by electrodialysis following chemical precipitation. Sep Sci Technol 39(7):1501–1517. https://doi.org/10.1081/SS-120030788

Redlich O, Peterson DL (1959) A useful adsorption isotherm. J Phys Chem 63(6):1024–1024. https://doi.org/10.1021/j150576a611

Sakai K, Okada K, Uka A, Misono T, Endo T, Sasaki S, Abe M, Sakai H (2015) Effects of water on solvation layers of imidazolium-type room temperature ionic liquids on silica and mica. Langmuir 31(22):6085–6091. https://doi.org/10.1021/acs.langmuir.5b01184

Samuel MS, Shah SS, Subramaniyan V, Qureshi T, Bhattacharya J, Singh NP (2018) Preparation of graphene oxide/chitosan/ferrite nanocomposite for chromium (VI) removal from aqueous solution. Int J Biol Macromol 119:540–547. https://doi.org/10.1016/j.ijbiomac.2018.07.052

Sanchez-Hachair A, Hafmann A (2018) Hexavalent chromium quantification in solution: Comparing direct UV-visible spectrometry with 1,5-diphenylcarbazidecolorimetry. C R Chimie 21:890–896. https://doi.org/10.1016/j.crci.2018.05.002

Shahwan T, Abu Sirriah S, Nairat M, Boyacı E, Eroğlu AE, Scott TB, Hallam KR (2011) Green synthesis of iron nanoparticles and their application as a fenton-like catalyst for the degradation of aqueous cationic and anionic dyes. Chem Eng J 172(1):258–266. https://doi.org/10.1016/j.cej.2011.05.103

Shariati S, Khabazipour M, Safa F (2017) Synthesis and application of amine functionalized silica mesoporous magnetite nanoparticles for removal of chromium(vi) from aqueous solutions. J Porous Mater 24(1):129–139. https://doi.org/10.1007/s10934-016-0245-5

Shariati S, Chinevari A, Ghorbani M (2020) Simultaneous removal of four dye pollutants in mixture using amine functionalized Kit-6 silica mesoporous magnetic nanocomposite. SILICON 12(8):1865–1878. https://doi.org/10.1007/s12633-019-00288-1

Sing KS, Williams RT (2004) Physisorption hysteresis loops and the characterization of nanoporous materials. Adsorp Sci Technol 22(10):773–782

Singh AK (2016) Chapter 8 - Nanoparticle Ecotoxicology. In: Singh AK (ed) Engineered Nanoparticles. Academic Press, Boston, pp 343–450

Spiess A-N, Neumeyer N (2010) An evaluation of R^2 as an inadequate measure for non-linear models in pharmacological and biochemical research: a monte carlo approach. BMC Pharmacol 10:6. https://doi.org/10.1186/1471-2210-10-6

Spigno G, De Faveri DM (2009) Microwave-assisted extraction of tea phenols: a phenomenological study. J Food Eng 93(2):210–217. https://doi.org/10.1016/j.jfoodeng.2009.01.006

Srivastava V, Sharma YC (2013) Synthesis and characterization of Fe_3O_4@n-SiO_2 nanoparticles from an agrowaste material and its application for the removal of Cr(VI) from aqueous solutions. Water Air Soil Pollut. https://doi.org/10.1007/s11270-013-1776-x

Stefaniuk M, Oleszczuk P, Ok YS (2016) Review on nano zero-valent iron (nZVI): from synthesis to environmental applications. Chem Eng J 287:618–632. https://doi.org/10.1016/j.cej.2015.11.046

Toutounchi S, Shariati S, Mahanpoor K (2019) Synthesis of nano-sized magnetite mesoporous carbon for removal of reactive yellow dye from aqueous solutions. Appl Organomet Chem 33(9):4971–4982. https://doi.org/10.1002/aoc.5046

Toutounchi S, Shariati S, Mahanpoor K (2021) Application of magnetic ordered mesoporous carbon nanocomposite for the removal of Ponceau 4R using factorial experimental design. SILICON 13(5):1561–1573. https://doi.org/10.1007/s12633-020-00535-w

Vijayaraghavan K, Padmesh T, Palanivelu K, Velan M (2006) Biosorption of nickel (II) ions onto sargassum wightii: Application of two-parameter and three-parameter isotherm models. J Hazard Mater 133(1–3):304–308. https://doi.org/10.1016/j.jhazmat.2005.10.016

Wang X, Pehkonen S, Ray AK (2004) Removal of aqueous Cr (VI) by a combination of photocatalytic reduction and co-precipitation. Ind Eng Chem Res 43(7):1665–1672. https://doi.org/10.1021/ie030580j

Weber WJ, Morris JC (1963) Kinetics of adsorption on carbon from solution. J Sanit Eng Div 89(2):31–60

Xing Y, Chen X, Wang D (2007) Electrically regenerated ion exchange for removal and recovery of cr (VI) from wastewater. Environ Sci Technol 41(4):1439–1443. https://doi.org/10.1021/es061499l

Yoo B-Y, Hernandez SC, Koo B, Rheem Y, Myung NV (2007) Electrochemically fabricated zero-valent iron, iron-nickel, and iron-palladium nanowires for environmental remediation applications. Water Sci Technol 55(1–2):149–156. https://doi.org/10.2166/wst.2007.017

Zhang Y, Zhang S, Chung T-S (2015) Nanometric graphene oxide framework membranes with enhanced heavy metal removal via nanofiltration. Environ Sci Technol 49(16):10235–10242. https://doi.org/10.1021/acs.est.5b02086

Zhang S, Shi Q, Korfiatis G, Christodoulatos C, Wang H, Meng X (2020) Chromate removal by electrospun pva/pei nanofibers: adsorption, reduction, and effects of co-existing ions. Chem Eng J 387:124179. https://doi.org/10.1016/j.cej.2020.124179